Tuning Charge Transport at the Interface between Indium Phosphide and a Polypyrrole−Phosphomolybdate Hybrid through Manipulation of Electrochemical Potential

Carrie Daniels-Hafer, Meehae Jang, Shannon W. Boettcher, Robert G. Danner, and Mark C. Lonergan*

Department of Chemistry and The Materials Science Institute, University of Oregon, Eugene, Oregon 97403

Received: August 6, 2001; In Final Form: November 19, 2001

The temperature-dependent current−voltage and capacitance−voltage characteristics of interfaces between InP and a polypyrrole−phosphomolybdate hybrid material (PMH) are reported as a function of the redox potential, E_{PMH}, of the PMH (as controlled by its extent of oxidation or p-type doping level). The current−voltage characteristics of the interfaces are sensitive to E_{PMH} and can be controlled over a much wider range than possible with analogous InP|metal interfaces. For the n-InP|PMH interfaces, the ability to tune the current−voltage characteristics by controlling E_{PMH} stems from control over the interfacial potential barrier ϕ_b characteristically present at semiconductor interfaces. The spatially averaged ϕ_b from capacitance−voltage measurements shifts from 0.59 to 1.05 V with a shift in E_{PMH} from −0.05 to +0.99 V vs SCE, leading to an index of interface behavior of $S = d\phi_b/dE_{PMH} = 0.39$. For the n-InP|PMH interfaces, heterogeneous electron transfer is slower than at the semiconductor|metal interfaces: the transmission coefficient κ, describing the probability that a carrier with sufficient thermal energy to surmount ϕ_b will actually cross the interface, is observed to be 0.003, independent of E_{PMH} and less than the semiconductor|metal limit of $\kappa = 1$. For the p-InP|PMH interfaces, the extent to which the current−voltage characteristics can be controlled through manipulation of E_{PMH} depends on both ϕ_b and κ. The S value for the p-InP interfaces is nearly identical with that for the n-InP|PMH interfaces: the spatially averaged capacitance−voltage ϕ_b shifts from 0.83 to 0.49 V with a shift of E_{PMH} from −0.07 to +0.65 V vs SCE, leading to $S = 0.37$. Over the same range of E_{PMH}, the value of κ decreases from the range of 1−0.1 to the range 0.05−0.0001 as E_{PMH} increases, suggesting that the majority carrier transfer rate depends on the details of the electronic structure of the PMH. The S values and empirical ideality factors observed for both the n-InP and p-InP interfaces are inconsistent with classic interface state models describing Fermi-level pinning. Nearly all of the interfaces demonstrate characteristic signatures of a heterogeneous barrier potential, such as, (1) ideality factors greater than unity and a decreasing function of temperature and (2) disagreement between the ϕ_b extracted from capacitance−voltage and temperature-dependent current−voltage measurements (Richardson plots). The quantitative application of Tung's barrier inhomogeneity model and the influence of heterogeneity on the extraction of κ and ϕ_b are discussed.

1. Introduction

This paper focuses on detailing the wide control possible over the current−voltage ($I-V_{app}$) characteristics of the interface between InP and the polypyrrole−phosphomolybdate hybrid material (PMH) formed from the oxidation of pyrrole by phosphomolybdic acid;[1,2] the control is achieved through electrochemical manipulation of the PMH to set its redox potential, E_{PMH}.[3] The understanding of charge-transfer processes at the InP|PMH and related inorganic semiconductor (IS)|doped conjugated polymer (DCP) interfaces is important to efforts to integrate molecular or macromolecular systems into conventional microelectronics.[3−8] These interfaces are also important bridges between more widely studied IS|metal[9−11] and IS|liquid redox couple[12−16] interfaces.

All of the above-mentioned interfaces belong to the important class of one-sided semiconductor interfaces formed from a nondegenerately doped IS contacted to another electroactive material that cannot support a substantial region of depleted charge, either due to a high density of mobile electrons or the presence of mobile ions. The substantial depletion region that does form in the IS is due to the ionization of a relatively low density of dopant atoms during charge-transfer equilibration. The electrostatic potential barrier ϕ_b created at such a depletion region and the limited charge carrier density present are useful, for instance, in gating current or in slowing carrier flux for the detailed study of heterogeneous electron-transfer kinetics.

As indicated above, the InP|PMH interface is an important bridge between IS|metal and IS|liquid redox couple systems. Interfaces between IS and metals (Schottky diodes) have been studied for over a century, and despite substantial effort, many basic aspects of these interfaces are still poorly understood, most notably the detailed origin of ϕ_b and its often weak dependence on the electrochemical potential $\bar{\mu}$ of the contact (Fermi-level pinning).[9−11] Interfaces between IS and liquid redox couples have been intensely investigated as photoelectrochemical cells for solar energy conversion, and their study has resulted in important contributions to our general understanding of heterogeneous electron-transfer kinetics.[14,17−20] Unlike IS|metal interfaces where the heterogeneous charge-transfer event is facile and independent of metal, the kinetics for charge transfer at IS|liquid redox couple interfaces exhibit much richer behavior and can be slower than with a metal contact.[13,21] Indeed, the fundamental relation between the heterogeneous charge-transfer rate and molecular or interfacial structure has been a key issue at such molecular IS interfaces.

10.1021/jp013022w CCC: $22.00
Published on Web 01/30/2002

The properties of PMH and conjugated polymers blend many aspects of metals and liquid redox couples, making IS interfaces based on them unique platforms for studying fundamental issues regarding charge transfer and charge equilibration. Like metals, PMH and related conjugated polymers are solid-state systems; this enables interrogation over a wide range of temperatures and with a wide variety of techniques. Moreover, analogous to liquid redox couples, they are molecular systems with lower dimensional bonding than metals; this enables the potential for reduced interfacial reactivity, active control of redox potential E (equivalently $\bar{\mu}$), and the study of charge transfer to localized electronic systems.

The wide range of control over $\bar{\mu}$ possible with PMH and DCPs is particularly important because of the central role $\bar{\mu}$ plays in "ideal" theories describing the origin of ϕ_b at one-sided IS interfaces. Unlike with metal contacts, where the relation of ϕ_b to $\bar{\mu}$ can only be studied by fabricating a series of different contacts, the dependence on $\bar{\mu}$ can be evaluated at a single interface through in situ electrochemical manipulation if PMH or a DCP is used. For PMH, it is possible to control E_{PMH} by more than 1 V and still have a good conductor ($\sigma \approx 1\ \Omega^{-1}\ cm^{-1}$). Our previous studies have exploited in situ tuning of E_{PMH} to demonstrate remarkable control over the current−voltage characteristics of the n-InP|PMH interface.[3] The range of current−voltage characteristics possible at this single interface is greater than can be achieved at all n-InP|metal interfaces combined. Herein we present a comprehensive study of majority carrier transport in the InP|PMH system using a series of interfaces electrochemically equilibrated at a particular E_{PMH} and then removed from the electrochemical cell for characterization in the solid state. This is done in order to more fully explore the dependence of the electrical characteristics of InP|PMH interfaces on E_{PMH}.

Thermionic emission (TE) theory[22] forms the basis for understanding the dependence of current on E_{PMH}. For ideal TE of carriers over a uniform temperature- and voltage-independent barrier, the equilibrium exchange current density J_o describing the magnitude of the carrier flux from the IS to the contact (and vice versa) at the point of dynamic equilibrium ($V_{app} = 0$) is given by

$$J_o = \kappa A^* T^2 \exp(-\beta\phi_b) \quad (1)$$

where A^* is a collection of material constants for the IS (60 A $K^{-2}\ cm^{-2}$ for p-type and 9.5 A $K^{-2}\ cm^{-2}$ for n-type InP),[9,23] κ is the transmission coefficient, and $\beta = q/(k_B T)$, where q is the electronic charge, k_B is the Boltzmann constant, and T is the absolute temperature. The barrier ϕ_b determines the fraction of carriers with sufficient thermal energy to surmount the interfacial potential barrier and reach the interface, while κ is the probability that carriers reaching the interface will indeed cross. For IS|metal interfaces, the heterogeneous charge transfer event is sufficiently facile that κ is generally taken as unity.[9−11] For more localized liquid redox couple systems, however, κ can be much less than unity.[13,21]

Equation 1 implies that any observed shift in current with E_{PMH} could be in part due to changes in κ or ϕ_b. For example, a variation in κ by a factor of 2 has the same effect on the current as a change in ϕ_b of approximately $k_B T/q$ (or ∼26 mV at 298 K). Therefore, this study analyzes the influence of E_{PMH} on both κ and ϕ_b. In general, the extraction of these parameters can be difficult due to deviations from ideal TE. In previous studies on the interface between n-InP and PMH that had not been electrochemically manipulated ("as-synthesized", $E_{PMH} =$ 0.4 V vs SCE), barrier heterogeneity did lead to deviations from ideal TE, but it was still possible to extract both ϕ_b and κ.[24] Herein, barrier inhomogeneity limits the precision with which these parameters can be determined.

At the outset, it is important to note that our previous studies have referred to PMH as "polypyrrole", or more specifically, as the polymer formed from the oxidation of pyrrole by phosphomolybdic acid.[3,24,25] Initial reports on this material did not indicate or rule out the incorporation of the phosphomolydate anion as an integral component of the molecular structure of this material.[1] Later studies by Gomez-Romero and Lira-Cantu[2] provided evidence for the phosphomolybdate anion as an integral part of the molecular structure and indicated that PMH is best regarded as a hybrid inorganic/organic material with on average nine pyrrole monomer units per phosphomolybdate anion.[26] For the redox potential range studied in this paper, the PMH is in its oxidatively or p-doped state with $\sigma \approx 1\ \Omega^{-1}\ cm^{-1}$, independent of E_{PMH}. Note that the terms n-type and p-type below refer only to the doping type of the InP.

The remainder of this paper is organized as follows. Section 2 outlines the experimental procedures used to construct and characterize the PMH interfaces. Section 3 presents current density−voltage ($J-V_{app}$) and capacitance−voltage ($C-V_{app}$) characteristics of both n-InP|PMH and p-InP|PMH interfaces as a function of E_{PMH}. Here, ideal TE theory forms the basis for our analysis and apparent values of κ and ϕ_b are calculated from different techniques. Section 3 also contains scanning electron microscopy (SEM) results from a cross-sectioned InP|PMH interface. In section 4, the transport data and the meaning of the apparent values of κ and ϕ_b extracted from both $J-V_{app}$ and $C-V_{app}$ methods are discussed in terms of a heterogeneous potential barrier. The tuning behavior seen at the InP|PMH interface is then discussed in terms of the relative dependencies of ϕ_b and κ on E_{PMH}. Furthermore, the relation of these dependencies to common Fermi-level pinning models and the density of states profile of PMH are discussed. Finally, the quantitative modeling of these interfaces with Tung's barrier inhomogeneity model[27] is presented in section 4.6.

2. Experimental Section

2.1. Materials. Prior to use, acetonitrile (Aldrich) was degassed by using three freeze−pump−thaw cycles, and pyrrole (Aldrich) was vacuum distilled. Tetrabutylammonium tetrafluoroborate (Bu_4NBF_4, Aldrich) was recrystallized from methanol and dried in vacuo (<20 mTorr) at 80 °C for 14 days. Methanol (Fisher), bromine (Fisher), silver nitrate (Sigma), ammonium hydroxide (J. T. Baker), and anhydrous tetrahydrofuran (Aldrich) were used as received. Polished indium phosphide wafers were purchased from Crystacomm, Inc., with Zn-doped p-type (100) wafers having an acceptor density of $N_A = 4.3 \times 10^{16}\ cm^{-3}$ and nominally undoped n-type (100) wafers having a donor density of $N_D = 5.2 \times 10^{15}\ cm^{-3}$. Gold minigrid (60 μm wire diameter, 250 μm spacing, 65% open) was purchased from Goodfellow, Inc. Ga/In eutectic was prepared by mixing equal amounts of gallium splatter (2.4 mm, Alfa) and indium shot (4 mm, Alfa) at room temperature.

2.2. Interface Fabrication. A schematic cross-section of the interface fabricated for these studies is shown in an expanded view in Figure 1. Back ohmic contacts were made to p-InP by sequential evaporation of ≈250 Å of Zn and ≈400 Å of Au followed by annealing in vacuo for 20 min in a 400 °C tube furnace, as reported by Kuphal.[28] The evaporated metal was then contacted with a Sn−Cu wire coil and silver print. A nonconducting epoxy cap was used to hold the wire in place. Ohmic contacts to the n-InP samples were made by using Ga/

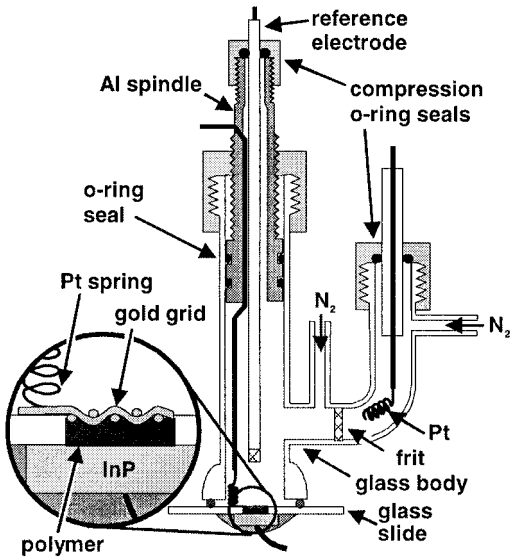

Figure 1. Cross-sectional schematic of the cell used for the electrochemical manipulation of IS|conjugated polymer interfaces. The region of the semiconductor interface is shown in an expanded view.

In eutectic contacted with a Sn−Cu wire coil stabilized with epoxy. The fabrication and etching procedures were identical with those previously described for studies on n-InP.[25] The PMH was synthesized by chemical oxidation of pyrrole by phosphomolybdic acid hydrate and cast from solution by the method described by Freund and co-workers.[1] For the p-InP|PMH interfaces, a PMH film was layered onto the surface of the semiconductor by sequentially casting drops of a reaction solution containing 0.165 g (∼0.09 mmol) of phosphomolybdic acid hydrate, 12.5 μL (0.18 mmol) of pyrrole in 1.10 mL of tetrahydrofuran. For n-InP|PMH interfaces, the reaction solution consisted of 0.165 g (∼0.09 mmol) of phosphomolybdic acid hydrate, 12.5 μL (0.18 mmol) of pyrrole in 0.55 mL of tetrahydrofuran. Although the reaction solution for the n-InP|PMH interfaces was more concentrated, the only differences observed in the electrical characteristics of the interfaces were due to the extent of PMH oxidation.

After a film was formed on the semiconductor surface, a gold grid current contact was positioned on top of the film and additional drops were cast through the grid to embed it. It should be noted that after casting, the PMH is insoluble to later casting drops, which prevents direct contact between the gold grid and the semiconductor surface. After casting, the interface was washed in methanol to remove any small molecule products of the polymerization and then dried in air. The interface was then transferred to the antechamber of an inert atmosphere glovebox (Vac Atmospheres, $\leq$5 ppm O_2) where subsequent manipulations were carried out under nitrogen.

The InP|PMH interface was clamped to an electrochemical cell, as shown in Figure 1, by using a standard O-ring seal and a Kalrez O-ring (Dupont Dow Elastomers). A standard glass frit separated two-compartment cell was used with a Pt coil counter electrode in one compartment and the PMH exposed semiconductor interface and a nonaqueous $Ag/AgNO_3$ reference electrode in the other. The electrolyte used was 0.10 M Bu_4NBF_4 in CH_3CN for p-InP|PMH and 0.12 M Bu_4NBF_4 in CH_3CN for n-InP|PMH interfaces. The PMH was electrically contacted by a Pt spring that was compressed onto a tail that extended from the gold grid ohmic contact embedded in the PMH. The potential of the $Ag/AgNO_3$ reference electrode was measured relative to a commercial saturated calomel electrode (SCE, Fisher Scientific), and all electrode potentials are reported vs SCE.

The PMH was driven to the desired potential with the gold grid as the working electrode of a conventional three-electrode arrangement using a Solartron 1287 potentiostat/galvanostat. The PMH was driven until the potential of the film was relatively stable in the absence of potentiostatic control, as evidenced by the stability of the $J-V_{app}$ curves. By the end of this period, the electrolysis current had dropped to nearly constant background levels. Current−voltage curves were collected intermittently during the driving process to verify the reproducibility of the $J-V_{app}$ characteristics at each E_{PMH} by using the back ohmic contact and gold grid as leads. After driving, the electrolyte was removed from the cell, and the interface was rinsed with CH_3CN to remove any excess salt. The interface was then placed into a steel airtight canister and evacuated (∼0.30 mTorr) for subsequent detailed electrical characterization.

Current measurements were made with a Keithley 236 Source Measure Unit. Capacitance−voltage measurements were made with a Solartron 1260 impedance analyzer over a frequency range of 10 Hz to 1 MHz with a 10 mV waveform amplitude. Temperature was controlled by placing the evacuated steel container in a Sun Systems environmental chamber.

2.3. SEM Characterization. The scanning electron microscopy (SEM) of the fabricated interfaces was carried out in a JEOL JSM-6300XV scanning electron microscope equipped with an Oxford Instruments eXL energy-dispersive X-ray detector (EDX). A 10 kV accelerating voltage was used. Prior to microscopy, samples were encased in epoxy, cross-sectioned, and then polished. An Edwards E306A was used for carbon evaporation onto the sample after polishing was complete.

3. Results

3.1. Current Density−Voltage ($J-V_{app}$) Characterization. Figure 2 shows current density−voltage ($J-V_{app}$) curves as a function of E_{PMH} for both n-InP|PMH and p-InP|PMH interfaces. The curves are for $T = 248$ K rather than room temperature because a slightly reduced temperature is required for a consistent treatment of all of the electrical measurements, as discussed further below. In our earlier report on the n-InP|PMH interface,[3] measurements as a function of E_{PMH} were performed on a single interface while it was immersed in an electrochemical cell. In contrast, each of the curves in Figure 2 was collected on a separate interface that had been equilibrated at a particular E_{PMH} and then removed from the electrochemical cell for characterization.

As is characteristic of IS interfaces, the InP|PMH interface is rectifying: the current is exponentially dependent on voltage for one sign of the applied bias, and weakly dependent on voltage for the other. The sign convention used in this paper places forward bias, corresponding to the flow of majority carriers (holes for p-type and electrons for n-type) from the IS to the PMH, at positive applied potentials.

As reported earlier, the $J-V_{app}$ curves for the n-InP|PMH interface shift toward higher applied voltage as E_{PMH} increases. The p-InP|PMH interfaces mirror this shift with the $J-V_{app}$ curves moving toward lower applied potential as E_{PMH} increases. The magnitude of the shift with E_{PMH} is somewhat smaller for the p-InP|PMH interfaces than for the n-InP|PMH interfaces. At a constant current density of 0.5 mA cm^{-2}, the current−voltage curves shift 0.45 V in response to a 1.04 V change in E_{PMH} for n-InP and 0.24 V in response to a 0.72 V change in E_{PMH} for p-InP. To address the issue of reversibility, both an

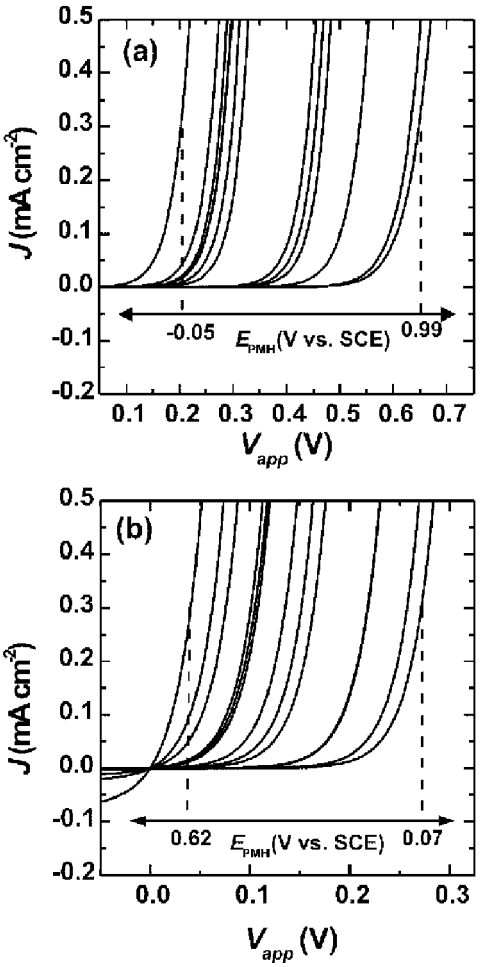

Figure 2. Current density−voltage ($J-V_{app}$) curves for (a) n-InP|PMH and (b) p-InP|PMH interfaces as a function of E_{PMH} at $T = 248$ K. In (a), the far right trace is for $E_{PMH} = -0.05$ V vs SCE, with the next twelve traces to the left being a result of incremental positive shifts in E_{PMH} up to 0.99 V vs SCE. In (b), the far right trace is for $E_{PMH} = 0.07$ V vs SCE, with the next twelve traces to the left being a result of shifts in E_{PMH} up to 0.62 V vs SCE.

n-InP|PMH and p-InP|PMH interface were fully characterized at a particular E_{PMH}, driven away from this initial E_{PMH}, and then driven back with good overlap of the $J-V_{app}$ curves.

Figure 3 contrasts n-InP|PMH and p-InP|PMH interfaces with similar barrier heights (the measurement of which will be described below) in a semilogarithmic plot to provide a more complete picture of the $J-V_{app}$ characteristics. The semilogarithmic n-InP|PMH curve is an example of the most complex behavior observed. In strong forward bias ($\beta V_{app} > 3$), there are two nearly linear portions of the semilogarithmic $J-V_{app}$ curve as well as curvature at high J. The curvature at high J is due to series resistance from contact wires and/or bulk resistance of the IS and PMH. Multiple linear regions in semilogarithmic $J-V_{app}$ curves are generally observed when there are multiple competing mechanisms for charge transport. As will be detailed below, the higher current linear portion of the $J-V_{app}$ curves depends on temperature and the ϕ_b characterizing the interface. These observations are consistent with carrier transport by TE of majority carriers, and when this mechanism dominates, the $J-V_{app}$ data can be used to interrogate ϕ_b and κ. As these are the primary parameters of interest, we focus on the higher current linear portion of the $J-V_{app}$ curves. For the current density range shown in the linear representation of Figure 2 ($\approx$0.5 mA cm^{-2}), TE dominates the observed current. The nature

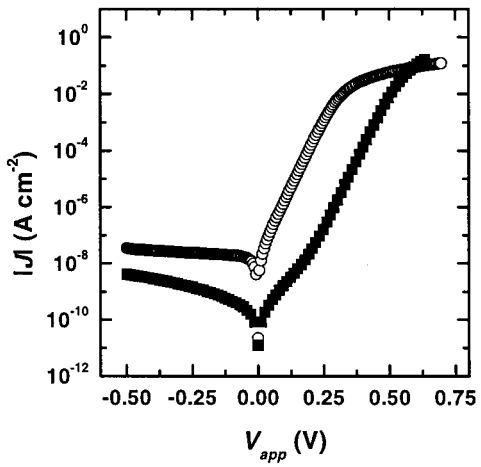

Figure 3. Absolute current density $|J|$ as a function of applied bias V_{app} for a representative n-InP|PMH (n7, solid squares, $\phi_b^{CV} = 0.73$) and p-InP|PMH (p3, open circles, $\phi_b^{CV} = 0.74$) interface with similar barrier heights at $T = 248$ K. Two linear portions of the forward bias ($V_{app} > 0$) current can be seen for interface n7; this paper will focus on the linear region at higher applied bias. Curvature at higher forward bias is attributed to series resistance.

of the secondary current mechanism has not been identified, and it is observed to be largely independent of T and ϕ_b.

For our subsequent analysis, it is convenient to introduce a scaled current density J' and two empirical parameters, n_{emp} and J_θ, that can be used to represent $J'-V_{app}$ curves in a compact manner.[10] The scaled current density J' is defined as

$$J' = \frac{J}{[1 - \exp(-\beta V_{app})]} \tag{2}$$

The current density J is equivalent to J' under strong forward bias ($\beta V_{app} > 3$). The usefulness of J' comes from the fact that the $J-V_{app}$ relation for an IS interface can often be written in the following form:

$$J = C[\exp(\beta V_{app}) - 1] \tag{3}$$

where C is a characteristic current density which may be dependent on V_{app}. In ideal TE theory, C equals J_o from eq 1 and is independent of V_{app}. When C is independent of V_{app}, a semilogarithmic plot of J' vs V_{app} will be linear, allowing for the consistent treatment of the negative reverse bias current together with the positive forward bias current. This is particularly useful when series resistance complicates analysis of the strongly forward bias region. Furthermore, it can be observed that J' approaches J_o as $V_{app} \rightarrow 0$, whereas J approaches zero as $V_{app} \rightarrow 0$.

A compact way to represent a $J'-V_{app}$ curve is through the empirical parameters n_{emp} and J_θ, where

$$n_{emp} = \left(\frac{1}{\beta}\frac{d \ln J'}{dV_{app}}\right)^{-1} \tag{4}$$

$$\ln J_\theta = \ln J' - \beta V_{app} \tag{5}$$

The parameter n_{emp} is related to the slope of a $\ln J'-V_{app}$ curve, with a larger n_{emp} signaling a weaker dependence of J' on an applied bias, while the parameter J_θ is related to the current at a particular reference voltage. For ideal TE theory, $n_{emp} = 1.00$ and $J_\theta = J_o$. Note that a more common approach to analyzing current voltage curves is to calculate an apparent exchange current density by extrapolation of a tangent line to the $J-V_{app}$

TABLE 1: Parameters Characterizing the Electrical Properties of n-InP|PMH Interfaces[a]

interface no.	E_{PMH} (V)	J' range (A cm^{-2})	n_{emp} 248 K	n_{emp} 123 K	$J_{\theta,248K}$ (A cm^{-2})	$\bar{V}_{248K}$ (V)	$q\phi^{RP}_{b,\theta,248K}$ (eV)	$q\phi^{CV}_{b,248K}$ (eV)	α (10^{-4} V K^{-1})	$\log \kappa^{CV}_{\theta,248K}$	$\log \kappa^{RP}_{\theta,248K}$
n1	−0.05	10^{-7}−10^{-4}	1.10	1.38	1.0×10^{-09}	0.19	0.60	0.59	−1.5	−2.7	−3.3
n2	0.09	10^{-5}−10^{-4}	1.10	*b*	2.2×10^{-11}	0.30	0.76	0.69	−3.2	−2.4	−2.5
n3	0.09	10^{-6}−10^{-4}	1.07	1.28	8.7×10^{-12}	0.30	0.76	0.71	−2.3	−2.3	−2.6
n4	0.12	10^{-6}−10^{-4}	1.14	1.49	4.4×10^{-12}	0.31	0.80	0.74	−2.9	−2.1	−2.3
n5	0.14	10^{-6}−10^{-4}	1.05	1.14	1.0×10^{-11}	0.29	0.75	0.70	−2.4	−2.6	−2.7
n6	0.30	10^{-6}−10^{-4}	1.06	1.17	4.1×10^{-12}	0.31	0.78	0.73	−2.5	−2.4	−2.5
n7	0.35	10^{-5}−10^{-3}	1.06	1.20	1.1×10^{-12}	0.39	0.82	0.75	−2.3	−2.4	−2.3
n8	0.56	10^{-5}−10^{-3}	1.19	1.35	5.6×10^{-15}	0.50	0.91	0.85	−2.4	−2.7	−2.7
n9	0.69	10^{-6}−10^{-5}	1.08	1.30	3.4×10^{-15}	0.44	0.93	0.89	−2.8	−2.1	−2.7
n10	0.76	10^{-6}−10^{-4}	1.12	1.42	1.7×10^{-15}	0.47	0.92	0.91	−2.4	−2.1	−3.1
n11	0.91	10^{-5}−10^{-4}	1.23	*b*	9.7×10^{-17}	0.56	1.01	0.95	−3.2	−2.5	−3.0
n12	0.97	10^{-7}−10^{-5}	1.48	1.34	1.7×10^{-18}	0.56	1.11	1.05	−3.6	−2.2	−2.8
n13	0.99	10^{-7}−10^{-5}	1.21	1.37	2.5×10^{-18}	0.56	1.10	1.03	−3.4	−2.4	−2.7

[a] Errors are estimated to be ±0.01 for n_{emp}, ±0.03 for $\phi^{RP}_{b,\theta}$, ±0.02 for ϕ^{CV}_{b}, ±0.4 for $\log \kappa^{CV}_{\theta}$, and ±0.6 for $\log \kappa^{RP}_{\theta}$. [b] *JV* curves were not collected at these temperatures.

TABLE 2: Parameters Characterizing the Electrical Properties of p-InP|PMH interfaces[a]

interface no.	E_{PMH} (V)	J' range (A cm^{-2})	n_{emp} 248 K	n_{emp} 123 K	$J_{\theta,248K}$ (A cm^{-2})	$\bar{V}_{248K}$ (V)	$q\phi^{RP}_{b,\theta,248K}$ (eV)	$q\phi^{CV}_{\theta,248K}$ (eV)	α (10^{-4} V K^{-1})	$\log \kappa^{CV}_{\theta,248K}$	$\log \kappa^{RP}_{\theta,248K}$
p1	−0.07	10^{-6}−10^{-4}	1.07	1.14	5.3×10^{-10}	0.20	0.81	0.83	−3.1	1.0	−0.9
p2	−0.07	10^{-7}−10^{-4}	1.09	*b*	1.7×10^{-9}	0.16	0.77	0.76	−3.0	0.1	−1.2
p3	0.03	10^{-7}−10^{-4}	1.04	1.11	8.5×10^{-9}	0.18	0.72	0.74	−2.9	0.5	−1.6
p4	0.03	10^{-7}−10^{-5}	1.04	1.12	1.4×10^{-8}	0.09	0.74	0.68	−1.4	−0.6	−0.1
p5	0.22	10^{-6}−10^{-3}	1.05	1.11	2.2×10^{-7}	0.10	0.62	0.64	−3.5	−0.3	−2.5
p6	0.22	10^{-7}−10^{-4}	1.06	1.10	1.3×10^{-7}	0.06	0.62	0.66	−3.2	0.0	−2.5
p7	0.43	10^{-6}−10^{-4}	1.03	1.14	6.7×10^{-7}	0.06	0.69	0.58	−0.5	−0.9	0.9
p8	0.43	10^{-6}−10^{-4}	1.08	1.15	2.3×10^{-6}	0.03	0.56	0.58	−2.7	−0.4	−2.2
p9[c]	0.51	10^{-5}−10^{-3}	1.08	1.36	2.4×10^{-6}	0.09	0.54	0.55	−2.8	−1.0	−3.5
p10[c]	0.55	10^{-7}−10^{-4}	1.04	1.10	3.1×10^{-6}	0.00	0.53	0.54	−2.6	−1.0	−3.6
p11	0.62	10^{-6}−10^{-4}	1.03	1.19	5.3×10^{-5}	−0.04	0.45	0.49	−5.1	−0.8	−4.3
p12	0.63	10^{-6}−10^{-4}	1.04	1.12	1.7×10^{-5}	−0.01	0.58	0.49	−1.4	−1.3	−0.3
p13[c]	0.65	10^{-6}−10^{-4}	1.05	1.21	8.7×10^{-6}	0.09	0.48	0.51	−2.3	−1.3	−4.5

[a] Errors are estimated to be ±0.01 for n_{emp}, ±0.03 for $\phi^{RP}_{b,\theta}$, ±0.02 for ϕ^{CV}_{b}, ±0.4 for $\log \kappa^{CV}_{\theta}$, and ±0.6 for $\log \kappa^{RP}_{\theta}$. [b] *JV* curves were not collected at these temperatures. [c] The lower temperature range for n_{emp} was 123 K.

curve to $V_{app} = 0$ V. The relation between this approach and the J_θ approach is discussed elsewhere.[29]

Tables 1 and 2 list the values of n_{emp} and J_θ for the interfaces studied at $T = 248$ K. Any slight curvature in a semilogarithmic $J'-V_{app}$ curve can lead to n_{emp} dependent on voltage, and for $n_{emp} \neq 1.00$, J_θ is voltage dependent. Consequently, the average voltages, $\bar{V}$, at which n_{emp} and J_θ were calculated are also tabulated. Consistent with its definition, J_θ shifts with E_{PMH} in a manner paralleling the shift in the $J-V_{app}$ curves shown in Figure 2. The highest values of n_{emp} for n-InP|PMH interfaces were observed at values of E_{PMH} furthest from the as-synthesized value of $E_{PMH} = 0.4 \pm 0.1$ V vs SCE. The change in n_{emp} was also seen to be reversible. For example, driving from 0.92 V vs SCE ($n_{emp} = 1.15(1)$) to −0.04 V vs SCE ($n_{emp} = 1.26(1)$) and back to 0.92 V vs SCE ($n_{emp} = 1.12(1)$) for an n-InP|PMH interface was accompanied by a reversible change of 0.12 in the value of n_{emp}. For the p-InP|PMH interfaces, n_{emp} was observed to change little with E_{PMH}.

3.2. Determination of Barrier Height: Temperature-Dependent $J-V_{app}$ Measurements. The temperature dependence of the $J'-V_{app}$ curves was investigated to provide a measure of ϕ_b. Figure 4 shows the temperature dependence of the $J'-V_{app}$ curves for both a representative n-InP|PMH and p-InP|PMH interface. As expected by TE, the $J'-V_{app}$ curves shift toward higher V_{app} as the temperature is lowered. The shift, however, is less than predicted by ideal TE, as can be seen by comparison to the theoretical curves shown: the range of applied bias spanned by the theoretical curves is greater than the experimental curves.

The empirical parameters n_{emp} and J_θ more clearly quantify the nature of the deviation from ideal TE. Figure 5a shows the temperature dependence of n_{emp} for interfaces n5 and p5. For the interfaces shown, n_{emp} is very close to the ideal TE value of unity at high temperature and increases as the temperature is lowered. The increase in n_{emp} with decreasing temperature is characteristic of all but one of the interfaces studied. Figure 5b illustrates the temperature dependence of J_θ in the form of a Richardson plot (RP) of $\ln J_\theta T^{-2}$ vs T^{-1}, which can be viewed as a type of Arrhenius or activation plot. Ideal TE predicts such a plot to be linear. As can be seen, however, RPs based on J_θ for both n-InP|PMH and p-InP|PMH interfaces are slightly concave up. It is noted that for $n_{emp} \neq 1$, J_θ is voltage dependent, and hence, the form of the RP depends on the voltage at which J_θ is evaluated. As it is not possible to measure J_θ at constant voltage due to the strong temperature dependence of TE, the RPs shown herein are always constructed with J_θ evaluated at a constant current density.

For transport governed by ideal TE, the slope of a RP can be used to calculate the barrier ϕ_b. According to eq 1

$$\phi_b^{RP} = -\frac{d[\ln(J_o/T^2)]}{d\beta} \qquad (6)$$

Here, the superscript RP is to emphasize that the barrier is calculated from a Richardson plot. For interfaces that do not rigorously agree with TE, as in Figure 4, it is only possible to calculate an apparent barrier, $\phi^{RP}_{b,\theta}$, from the replacement of J_o in eq 6 with J_θ. The fundamental significance of $\phi^{RP}_{b,\theta}$ will be

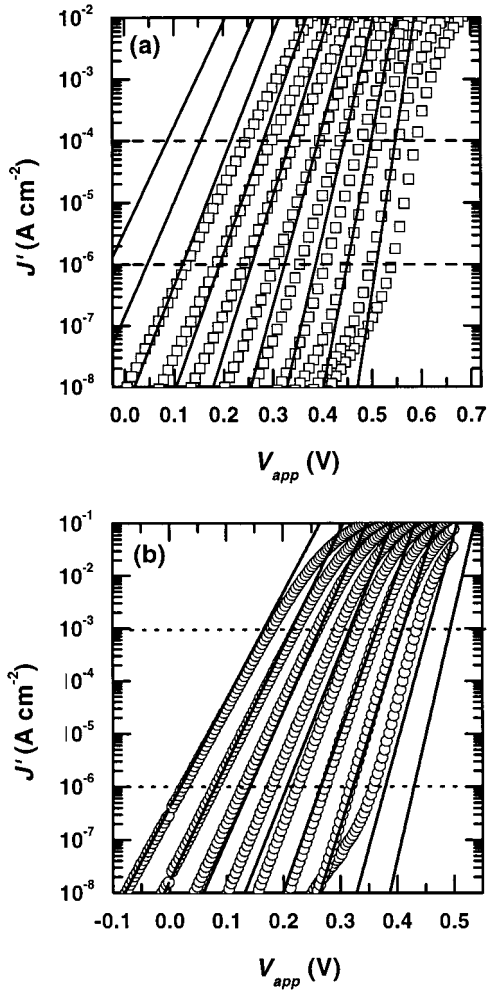

Figure 4. Temperature dependence of the reduced current density J' for (a) interface n5 (n-InP|PMH) with temperatures ranging from 98 to 298 K, stepped by 25 K, and for (b) interface p5 (p-InP|PMH) with temperatures ranging from 108 to 248 K, stepped by 20 K. Every other data point at each temperature is shown for clarity. The solid lines represent theoretical TE current density for a uniform interface based on eqs 1−3, assuming $C = J_o$, $\phi_b = \phi_b^{CV}$, and $\kappa = 1$. The horizontal lines bound the range of J' over which the modeling was undertaken.

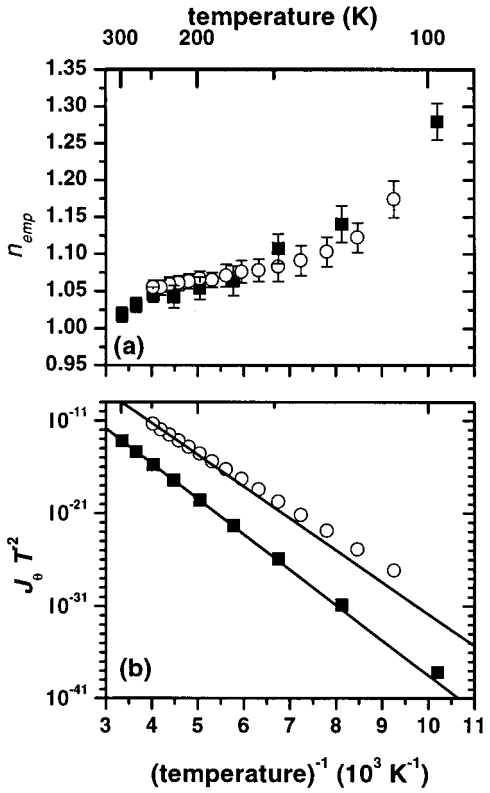

Figure 5. (a) Value of n_{emp} as a function of T^{-1} for interfaces n5 (n-InP|PMH, squares) and p5 (p-InP|PMH, circles) evaluated over a constant J' range (see Tables 1 and 2). (b) Semilogarithmic plot of $J_\theta T^{-2}$ vs T^{-1}, also known as a Richardson plot, for interfaces n5 (squares) and p5 (circles). The solid lines are fits to the high-temperature data and are the extrapolation expected from ideal TE with a temperature-independent barrier. The experimental error in $J_\theta T^{-2}$ is smaller than the symbols shown.

discussed in section 4.2. Figure 6 shows the temperature dependence of the apparent barrier $\phi_{b,\theta}^{RP}$ calculated from second-order polynomial fits to the RPs shown in Figure 5b. As can be seen, the apparent barrier decreases as the temperature is lowered for both the n-InP|PMH and p-InP|PMH interfaces shown. This behavior was characteristic of all of the interfaces studied.

The values of $\phi_{b,\theta}^{RP}$ calculated at $T = 248$ K for each of the interfaces studied are listed in Tables 1 and 2 along with the J' range over which they were calculated. The values of $\phi_{b,\theta}^{RP}$ increase linearly with increasing E_{PMH} with a slope of 0.38 ± 0.05 for the n-InP|PMH interfaces and decrease linearly with increasing E_{PMH} with a slope of -0.39 ± 0.04 for the p-InP|PMH interfaces.

3.3. Determination of Barrier Height−Capacitance−Voltage Characterization. Another common method used to measure ϕ_b is the capacitance−voltage ($C-V_{app}$) technique. The interfacial potential barrier ϕ_b^{CV} was extracted by reverse-biased $C-V_{app}$ measurements where the impedance of the interface was measured as a function of frequency. The capacitance was extracted from the region where the impedance, Z, was nearly purely capacitive (i.e., $|Z| = (\omega C)^{-1}$ and a phase

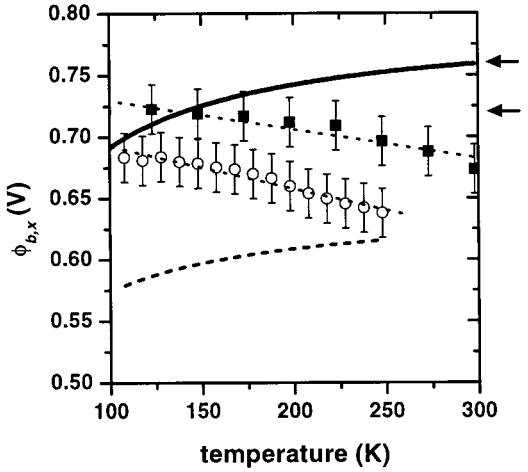

Figure 6. Barrier heights as a function of temperature for interfaces n5 (n-InP|PMH) and p5 (p-InP|PMH). The capacitance voltage barriers ϕ_b^{CV}, calculated as per Figure 7, are shown as solid squares (n-InP|PMH) and open circles (p-InP|PMH). The temperature-dependent $\phi_{b,\theta}^{RP}$, calculated by applying eq 6 to a second-order polynomial fit of the experimental Richardson plot data is shown as a solid line for n-InP|PMH and a dashed line for p-InP|PMH interfaces. The two barriers are consistent if $\phi_{b,\theta}^{RP}$ is equal to ϕ_b^{CV} extrapolated to $T = 0$ K. The values of $\phi_b^{CV}(T = 0$ K) based on linear extrapolations (dotted lines) of ϕ_b^{CV} are indicated by the upper (n5) and lower (p5) arrows.

angle between 86° and 90°). If there is no appreciable interfacial layer, the measured capacitance is the differential capacitance of the depletion layer:

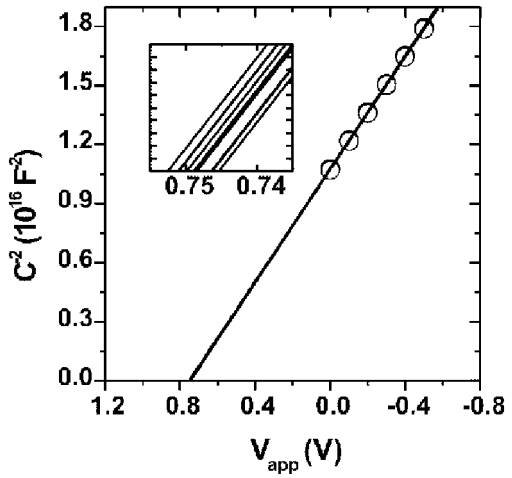

Figure 7. Plot of C^{-2} vs V_{app} for interface p2 at $T = 118$ K over a decade of frequencies. The linear regression fits are drawn to show the intercept on the bias axis, which are used to calculate the barrier height. The inset shows little spread of the horizontal axis intercepts, which imply the barrier height, as measured, is relatively independent of frequency.

$$\frac{1}{C^2} = \frac{2(V_{b0} - V_{app} - kT/q)}{q\epsilon_s NA^2} \tag{7}$$

where V_{b0} is the built-in potential, ϵ_s is the static dielectric constant of the IS, N is the impurity concentration of the IS, and A is the area.[10] A plot of C^{-2} versus V_{app} is linear, with the slope related to N, and the intercept with the V_{app} axis (at $C^{-2} = 0$), giving the quantity $V_{b0} - k_B T/q$. The $C-V_{app}$ measured barrier height is related to V_{b0} by

$$\phi_b^{CV} = V_{b0} + V_{n(p)} \tag{8}$$

where $qV_{n(p)}$ is the difference between the Fermi level and the valence (conduction) band edge in the bulk of the n-type (p-type) semiconductor. Figure 7 shows a representative plot of C^{-2} vs V_{app} for over an order of magnitude in frequency for the representative InP|PMH interface p2. The frequency dispersion in this plot is shown more clearly in the inset and is typical of all of the interfaces studied.

Near room temperature, the relatively high reverse bias current exhibited by most of the p-InP|PMH interfaces made extraction of ϕ_b^{CV} difficult because a large parallel conduction hinders the measurement of the depletion region capacitance. The highest temperature studied for which it was possible to extract ϕ_b^{CV} for all of the interfaces was $T = 248$ K. Therefore, this paper focuses on lower temperatures $T \leq 248$ K for both the n-InP|PMH and p-InP|PMH interfaces, as alluded to above.

The values of ϕ_b^{CV} at $T = 248$ K are listed in Tables 1 and 2 for each of the n-InP|PMH and p-InP|PMH interfaces studied, and the temperature dependence for representative interfaces is shown in Figure 6. In each case, the $C-V_{app}$ measurements accurately reproduced the dopant density of the InP, as is consistent with one-sided IS interface with a substantial depletion region only present in the InP. Also tabulated is the slope, α, of a linear fit to ϕ_b^{CV} as a function of T over the range 125−250 K. The extent to which the dependence of ϕ_b^{CV} on temperature is linear can be seen from the fits shown in Figure 6.

The dependence of ϕ_b^{CV} on E_{PMH} was similar to that observed for $\phi_{b,\theta}^{RP}$ at 248 K. A plot of ϕ_b^{CV} versus E_{PMH} for both n-InP|PMH and p-InP|PMH interfaces as well as a sum of these two functions is shown in Figure 8. The point of this figure is to illustrate that the barrier potential at the InP|PMH interface can be manipulated by changing E_{PMH}. A linear regression to the experimental data presented indicates that the magnitude of the slope, $|S|$, is equal to 0.39 ± 0.03 for p-InP|PMH interfaces and 0.37 ± 0.03 for the n-InP|PMH interfaces; the parameter $|S|$ is a measure of the control possible over the barrier potential and is useful for comparing mechanisms of Fermi-level pinning. The significance of this parameter, as well as the sum of ϕ_b^{CV} for both n-InP|PMH and p-InP|PMH interfaces will be discussed in sections 4.4.1 and 4.4.2. This dependence of ϕ_b^{CV} on E_{PMH} is reversible. For example, cycling from 0.75 V vs SCE ($\phi_b^{CV} = 0.93$ V) to 0.4 V vs SCE ($\phi_b^{CV} = 0.79$ V) and back to 0.75 V vs SCE ($\phi_b^{CV} = 0.93$ V) was accompanied by a reversible change of 0.14 V in the barrier height. Similar behavior was also observed in the p-InP|PMH interfaces.

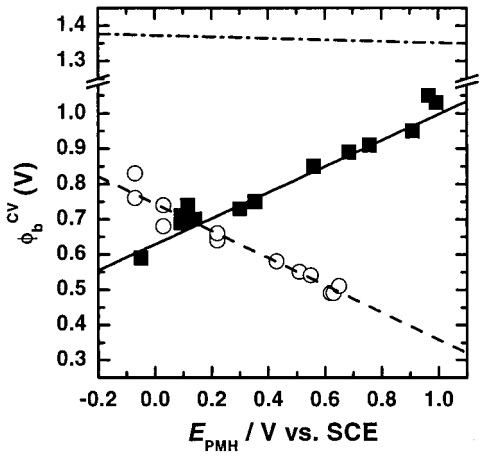

Figure 8. Barrier heights extracted using the capacitance−voltage method as a function of E_{PMH} for the n-InP|PMH (solid squares) and p-InP|PMH (open circles) interfaces. The symbol size roughly reflects the ± 0.02 V error. The solid line is a linear fit to the n-InP|PMH data, yielding an absolute slope of $|S| = 0.37 \pm 0.03$. The dashed line is a linear fit to the p-InP|PMH data, yielding an absolute slope of $|S| = 0.39 \pm 0.03$. The dash−dot line above represents a sum of the linear fits describing the n-InP|PMH and p-InP|PMH interfaces.

3.4. Calculation of κ_θ^{RP} and κ_θ^{CV}. Ideal TE theory provides a recipe for calculating κ from ϕ_b through eq 1:

$$\kappa = \frac{J_o}{A^* T^2} \exp(\beta\phi_b) \tag{9}$$

As with the RP barrier, it is only possible to define an apparent value of κ for an interface that does not rigorously agree with ideal TE. Furthermore, the different techniques used to measure the barrier may lead to different values. We define κ_θ^{RP} and κ_θ^{CV} as the apparent values from eq 9 with J_o replaced by J_θ and ϕ_b replaced by the appropriate barrier.

There is an additional subtlety in defining ϕ_b^{RP} because the use of eq 6 to calculate ϕ_b^{RP} requires the barrier to be independent of temperature. Contrary to this, the empirical values $\phi_{b,\theta}^{RP}$ and ϕ_b^{CV} are temperature-dependent, as shown in Figure 6. To deal with this complication, we introduce a first-order correction to ϕ_b^{RP} in the calculation of κ_θ^{RP}. For a barrier linearly dependent on temperature, the value of ϕ_b^{RP} calculated according to eq 6 is the barrier extrapolated to $T = 0$ K.[30,31] At finite temperature, then, the value of κ_θ^{RP} is explicitly related to $\phi_{b,\theta}^{RP}$ by

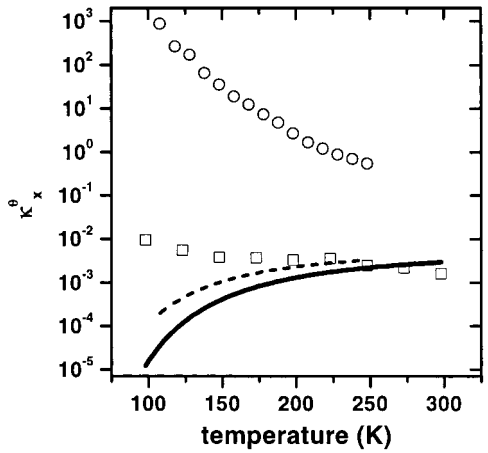

Figure 9. Comparison of κ_θ^{CV} and κ_θ^{RP} as a function of temperature. The open squares and solid line are κ_θ^{CV} and κ_θ^{RP}, respectively, for interface n5 (n-InP|PMH). The open circles and dashed line are κ_θ^{CV} and κ_θ^{RP}, respectively, for interface p5 (p-InP|PMH). For an interface with a uniform barrier, the values of κ_θ^{CV} and κ_θ^{RP} are expected to agree. The values of κ_θ^{RP} were calculated on the basis of a second-order polynomial fit to the Richardson plot data in Figure 5b. The errors are estimated to be ± 0.6 for log κ_θ^{RP} and ± 0.4 for log κ_θ^{CV}.

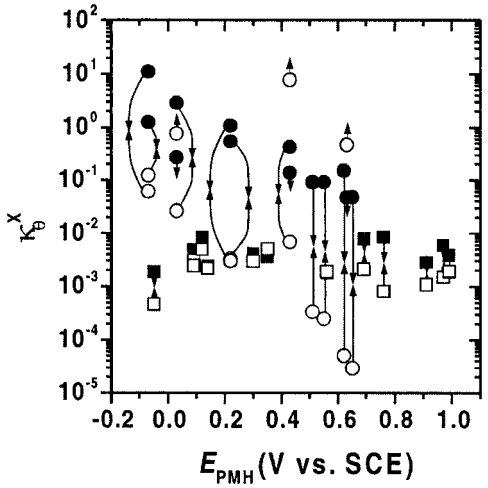

Figure 10. Comparison of κ_θ^{CV} and κ_θ^{RP} vs E_{PMH} for both the n-InP|PMH and p-InP|PMH interfaces at $T = 248$ K. The solid symbols represent the values of κ_θ^{CV} for the n-InP|PMH (squares) and the p-InP|PMH (circles) interfaces, and the open symbols represent the values of κ_θ^{RP} for the n-InP|PMH (squares) and the p-InP|PMH (circles) interfaces. The arrows tie together the upper limit, κ_θ^{CV}, and lower limit, κ_θ^{RP}, for each interface. The errors are estimated to be ± 0.6 for log κ_θ^{RP} and ± 0.4 for log κ_θ^{CV}.

$$\kappa_\theta^{RP} = \frac{J_\theta}{A^* T^2 \exp(-\beta\phi_{b,\theta}^{RP}) \exp(-q\alpha/T)} \qquad (10)$$

As the value of α cannot be extracted from RP measurements alone without independent knowledge of κ, we use the α derived from $C-V_{app}$ measurements in this correction. The validity of this approach in light of the apparently very different temperature dependencies of ϕ_b^{CV} and ϕ_b^{RP} will be discussed in section 4.2.

Figure 9 shows a comparison of the apparent values of κ_θ^{CV} and κ_θ^{RP} as a function of temperature. The value of κ_θ^{CV} is generally greater than κ_θ^{RP} for both the n-InP|PMH and the p-InP|PMH interfaces. Furthermore, the discrepancy between these values increases as the temperature is lowered. As with many of the interfaces studied, the interface shown has increasingly nonphysical (>1) values of κ_θ^{CV} as T is lowered.

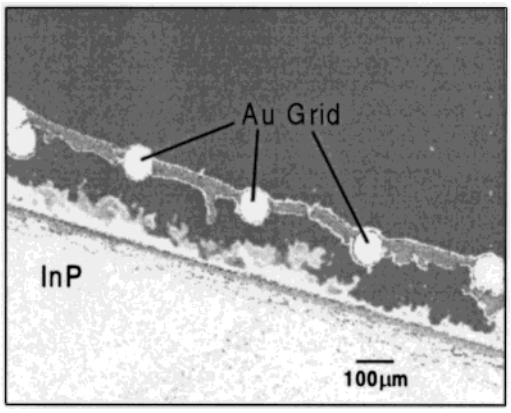

Figure 11. Scanning electron micrograph cross-section of an n-InP|PMH interface. The secondary electron image contains some backscattered component. The Au grid and InP substrate are indicated in the figure and bound a layer of PMH that is approximately 215 μm thick. X-ray spectral analysis data indicates Mo dispersed throughout the PMH, as expected, and a much higher content of Mo near each of the interfaces.

Apparent values of κ_θ^{CV} and κ_θ^{RP} for both n-InP|PMH and p-InP|PMH interfaces are given in Tables 1 and 2 for each E_{PMH} at $T = 248$ K, and Figure 10 shows a plot of these values. As above, κ_θ^{CV} is greater than κ_θ^{RP}, and in certain cases, the value of κ_θ^{CV} is observed to be greater than the theoretical limit of unity. Despite the substantial noise present, it can be seen that κ_θ^{RP} and κ_θ^{CV} are relatively independent of E_{PMH} for the n-InP|PMH interfaces and, on average, decrease as E_{PMH} increases for the p-InP|PMH interfaces.

3.5. Interface Structure. To investigate the possible role of interface structure on the current−voltage characteristics of these interfaces, scanning electron microscopy (SEM) was used to study electron density at the InP|PMH interface. Figure 11 shows a SEM micrograph of a cross-sectioned InP|PMH interface, indicating the presence of an electron rich layer at each of the surfaces present in the structure. Subsequent EDX characterization demonstrated the electron rich regions near the surfaces had a substantially increased Mo content relative to the bulk PMH. This suggests that the structure of the PMH in the vicinity of the interface is very different from the bulk composition described in the Introduction. This difference may arise from nucleation processes and could possibly indicate a substantial degree of interfacial reactivity. Such interfacial reactivity has implications for the Fermi-level pinning of these interfaces, as discussed in section 4.4.3.

4. Discussion

4.1. Background−Voltage-Dependent Barriers and the Meaning of n_{emp} and J_θ. Our discussion of current transport at the InP|PMH interface requires dealing with a voltage-dependent barrier. Consequently, we briefly consider ideal TE only complicated by a voltage-dependent barrier. In particular, we consider the meaning of n_{emp} and J_θ for this situation. A barrier that increases with increasing forward bias gives rise to $n_{emp} > 1$. For instance, combining eqs 1, 3, and 4 with $C = J_o$ yields $n_{emp} = [1 - d\phi_b/dV]^{-1}$ for a uniform barrier that depends linearly on applied bias. The quantity J_θ can also be understood in terms of a voltage-dependent barrier. When $n_{emp} > 1$, J_θ is not a true exchange current density describing the magnitude of the carrier flux from the IS to the contact (and vice versa) at the point of dynamic equilibrium ($V_{app} = 0$). For $n_{emp} > 1$ only

due to a voltage-dependent barrier, J_θ can be identified as a hypothetical exchange current density characterizing the interface with the barrier at a particular voltage hypothetically frozen out.[29] This can be seen by recognizing that eq 5 is the form of the $J-V_{app}$ curve for ideal thermionic emission (eq 3 with $C = J_o$), but with J_o replaced by J_θ. The $J-V_{app}$ curve for thermionic emission over a voltage-dependent barrier can be seen as crossing over a series of ideal $J-V_{app}$ curves each for a different barrier and an exchange current density given by J_θ. Hence, for ideal TE only complicated by a voltage-dependent barrier, J_θ can be treated just like the true exchange current density J_o, but it is emphasized that J_θ refers to the barrier at a finite voltage whereas J_o refers to the barrier at $V_{app} = 0$.

The identification of J_θ as a hypothetical exchange current density implies that $\phi_{b,\theta}^{RP}$ is a measure of the barrier height at a particular bias. A caveat is that this interpretation only rigorously holds for RPs constructed at constant voltage, which is not practical for reasons mentioned above. For a real RP constructed closer to the constant J condition, the meaning of $\phi_{b,\theta}^{RP}$ can become clouded if $(\partial\phi_b/\partial V_{app})_\beta$ $(dV_{app}/d\beta)$ is sufficiently strong. As discussed below, we consider a voltage-dependent barrier due to the bias dependence of the electrostatic potential profile about nanometer scale low-barrier defects. Model calculations based on Tung's model for such small defects demonstrate that $(\partial\phi_b/\partial V_{app})_\beta(dV_{app}/d\beta)$ is sufficiently small that $\phi_{b,\theta}^{RP}$ provides a fair measure of the true activation energy for carrier transport, and consequently, we interpret it as such below. It is important, however, to recognize the limitations of this interpretation and of RPs in general, as is discussed further below as well as elsewhere.[29]

4.2. Current Transport−Barrier Inhomogeneities and the Meaning of $\phi_{b,\theta}^{RP}$, ϕ_b^{CV}, κ_θ^{RP}, and κ_θ^{CV}. We hypothesize that carrier transport at the InP|PMH interface is characterized by a low spatial coverage of nanoscale low-barrier regions imbedded in an otherwise uniform voltage-independent barrier that weakly increases as the temperature decreases. For as-synthesized InP|PMH ($E_{PMH} = 0.4$ V vs SCE) interfaces, our previous work strongly supports this hypothesis,[24,25] and for the interfaces reported herein where E_{PMH} has been manipulated, the key signatures of a heterogeneous barrier potential are also present. Three such signatures are briefly discussed below; a more complete description in the context of the as-synthesized interfaces and competing models can be found elsewhere.[24,25] The discussion in the remainder of this section on current transport also clarifies the meaning of the apparent quantities defined in the Experimental Section.

4.2.1. Observation No. 1: n_{emp} Greater Than Unity and a Decreasing Function of Temperature. Nanometer scale barrier inhomogeneity provides a natural explanation for n_{emp} greater than unity and as a decreasing function of temperature (Figure 5). As discussed by Tung, the effective barrier of a small-scale low barrier region imbedded in a high-barrier background depends on voltage due to the interaction of its depletion region with that of the high-barrier background (potential "pinch-off").[27] Here, small scale refers to a lateral dimension smaller than the depletion width of the high-barrier background. As discussed in section 4.1, the voltage dependence of the effective barrier at a pinched-off patch gives rise to $n_{emp} > 1$ for carrier transport through it. The temperature dependence arises from how the barrier distribution is sampled with temperature. At sufficiently low temperature, carrier transfer will be localized to the low barrier patches and be characterized by $n_{emp} > 1$. At sufficiently high temperature, the background region will dominate. If the background barrier is uniform and voltage-independent as hypothesized for the InP|PMH interfaces, n_{emp} will approach unity at sufficiently high temperatures because the thermal energy will blur any heterogeneity and transport will be dominated by carrier transport through the background region. As the temperature is lowered, carrier transport will become increasingly localized to barrier inhomogeneities, and n_{emp} will increase due to the voltage dependence of the effective barrier at these so-called patches. Consistent with this, n_{emp} for all but one of the InP|PMH interfaces increases as the temperature is lowered (see Tables 1 and 2 and Figure 5). The one exception (n12) had among the highest ideality factors observed.

4.2.2. Observation No. 2: Increasing Divergence between $\phi_{b,\theta}^{RP}$ and ϕ_b^{CV} as the Temperature Is Lowered. Barrier heterogeneity also provides a natural explanation for discrepancies between various measures of the barrier height. For a heterogeneous barrier, capacitance−voltage techniques provide an area−weighted average,[32,33] whereas RP measurements provide a current−weighted average. At temperatures sufficiently high to blur any heterogeneity, ϕ_b^{CV} and $\phi_{b,\theta}^{RP}$ are expected to be equivalent. As the temperature is lowered, however, ϕ_b^{CV} and $\phi_{b,\theta}^{RP}$ are expected to diverge due to the different manner in which they weight the barrier distribution. The value of $\phi_{b,\theta}^{RP}$ will decrease as the temperature is lowered because the current becomes increasingly localized to low barrier regions. In contrast, ϕ_b^{CV} will only change if the barrier distribution itself changes rather than simply the way carrier transport samples it. In general, $\phi_{b,\theta}^{RP}$ is expected to be less than or equal to ϕ_b^{CV}.

Consistent with this picture, $\phi_{b,\theta}^{RP}$ at the InP|PMH interface is observed to decrease as the temperature is lowered (see Figure 6). At high temperature, however, ϕ_b^{RP} is often observed to be greater than ϕ_b^{CV}, which is not expected from a barrier inhomogeneity model. This apparent discrepancy can be resolved by considering an additional complication in the analysis of RPs, namely, any temperature dependence of the barrier. For a uniform barrier that depends linearly on temperature, $\phi_{b,\theta}^{RP}$ calculated according to eq 6 yields the 0 K barrier.[31] Consequently, agreement between ϕ_b^{CV} and $\phi_{b,\theta}^{RP}$ to signal a uniform barrier is expected to be in the form of $\phi_{b,\theta}^{RP}(T\rightarrow\infty) = \phi_b^{CV}(T=0$ K), where $\phi_{b,\theta}^{RP}$ is calculated according to eq 6. Figure 6 shows that $\phi_{b,\theta}^{RP}$ does indeed approach the linearly extrapolated value of $\phi_b^{CV}(T=0$ K) for the representative n-InP|PMH interface. For the p-InP|PMH interfaces the agreement between $\phi_{b,\theta}^{RP}(T=248$ K) and $\phi_b^{CV}(T=0$ K) is poorer than with the n-InP|PMH interfaces, indicating that heterogeneity may still be a problem for the p-InP|PMH interfaces even at the highest temperature studied ($T = 248$ K). The extent to which ϕ_b^{CV} truly depends linearly on temperature also effects this comparison.

4.2.3. Observation No. 3: κ_θ^{CV} κ_θ^{RP} and $\kappa_\theta^{CV} > 1$. In the presence of an inhomogeneous barrier, the true value of κ is bounded between an upper limit measured by the $C-V_{app}$ barrier and a lower limit measured by a RP barrier.[29] The spatially averaged ϕ_b^{CV} yields an upper limit because it overestimates the activation energy when the current is dominated by barrier inhomogeneities. In contrast, the current weighted $\phi_{b,\theta}^{RP}$ can yield an accurate activation energy for carrier transport, but the use of the geometric area in calculating J_θ leads to an underestimation in κ when carriers preferentially pass through barrier inhomogeneities covering only a small fraction of the interface.

As predicted, κ_θ^{CV} is observed to be greater than or equal (within experimental error) to κ_θ^{RP} for 23 of the 26 interfaces studied at $T = 248$ K. As the temperature is lowered, the discrepancy between κ_θ^{CV} and κ_θ^{RP} increases as carrier transport occurs preferentially through the low-barrier patches. In many cases, κ_θ^{CV} is often observed to exceed unity, and such nonphysical values are consistent with it representing an upper limit. Consistent with the notion that the n-InP|PMH interface behaves uniformly at $T = 248$ K, there is little discrepancy between κ_θ^{CV} and κ_θ^{RP} calculated for this interface (see Figure 9). For the p-InP|PMH interfaces, disagreement remains between ϕ_b^{CV} and $\phi_{b,\theta}^{RP}$, reflecting the presence of some heterogeneity. This is also reflected in the values of κ_θ^{CV} and κ_θ^{RP} which remain separated by an order of magnitude or two.

The presence of a heterogeneous barrier potential can also be used to rationalize the earlier correction of κ_θ^{RP} using the temperature dependence of ϕ_b^{CV}. An accurate κ can only be determined if the interface is behaving effectively uniform. Within our hypothesized heterogeneous barrier potential, this means that the uniform background barrier dominates transport. For a low spatial coverage of barrier inhomogeneities, the ϕ_b^{CV} measures the uniform barrier background, leading to its temperature dependence. The use of ϕ_b^{CV} in correcting the Richardson plot data is only valid at temperatures sufficiently high that the interface behaves effectively uniform. As we are primarily interested in this high-temperature limit, we applied a correction based on the temperature dependence of ϕ_b^{CV}. This correction and hence the value of κ_θ^{RP} become increasingly suspect as the temperature is lowered.

4.3. Origin of Tuning. As discussed in the Introduction, the control realized over the $J-V_{app}$ curves through manipulation of E_{PMH} could be due either to changes in κ or ϕ_b. At $T = 248$ K, Figure 10 illustrates the dependence of κ_θ^{CV} and κ_θ^{RP} (as upper and lower limits, respectively) on E_{PMH}. As shown, the κ characterizing the n-InP|PMH interfaces is not a strong function of E_{PMH}, remaining relatively constant at $\kappa = 0.003$ as E_{PMH} is manipulated. This indicates that the tuning observed with the n-InP|PMH interface is due almost exclusively to the dependence of ϕ_b on E_{PMH}. The primary role of ϕ_b can also be illustrated by directly comparing the shift in the $J-V_{app}$ curves with the shift in ϕ_b^{CV}. For ideal TE, the shift in the current−voltage curves should exactly parallel the shift in ϕ_b if κ is constant. Indeed, the $J-V_{app}$ curves, at a constant current density of 0.5 mA cm^{-2}, and ϕ_b^{CV} shift by nearly identical amounts (0.45 and 0.46 V, respectively) in response to a 1.04 V change in E_{PMH}. In contrast, for the p-InP|PMH interfaces, the $J-V_{app}$ curves, at a constant $J = 0.5$ mA cm^{-2}, shift less than ϕ_b^{CV} (0.24 and 0.36 V, respectively) in response to a 0.72 V change in E_{PMH}. It is tempting to attribute the smaller shift in the $J-V_{app}$ curves relative to ϕ_b^{CV} to a decrease in κ with E_{PMH}. The extent to which this is true is illustrated in Figure 10. The general trend for the p-InP|PMH interfaces is a decrease in κ from the range of 1−0.1 to the range 0.05−0.001 as E_{PMH} increases. The veracity of this assertion, however, is clearly influenced by the noise and complications due to heterogeneity, as evidenced by the separation between κ_θ^{CV} and κ_θ^{RP}. In other words, the extent to which the $J-V_{app}$ curves shift may not simply depend on κ and ϕ_b but also on contributions from heterogeneity. Regardless, the results for the p-InP|PMH interfaces demonstrate that the index of interface behavior S cannot necessarily be assessed from current−voltage curves alone because of the possibility for a simultaneous change in κ as well as ϕ_b. In the next two sections, more detailed discussions of the individual dependencies of κ and ϕ_b are given, and in section 4.6, the data are analyzed in terms of Tung's specific inhomogeneity model. To the extent to which the model holds, it is possible to assign a specific value of κ to each interface.

4.4. Dependence of ϕ_b on E_{PMH}. A complete understanding as to the origin of the barrier potential at an IS interface requires a microscopic picture that can describe not only the average barrier but also any heterogeneity present. Historically, discussions of Fermi-level pinning have focused on the *large-scale* influence of $\bar{\mu}$ on the average ϕ_b as expressed through the index of interface behavior S. For a heterogeneous interface, the spatially averaged ϕ_b^{CV} is most relevant to discussions focusing on the large-scale influence of $\bar{\mu}$ because the current-weighted $\phi_{b,\theta}^{RP}$ can be dominated by defects. The InP|PMH interfaces studied herein, however, behave sufficiently uniform at 248 K that the S values calculated from either the $C-V_{app}$ or RP barrier are the same. The average value of S for both techniques and for both n-InP|PMH and p-InP|PMH interfaces is 0.38 ± 0.3. In the remainder of this section, we discuss the experimentally observed value of $S = 0.38$ in terms of prevalent models describing the origin of the interfacial potential barrier at IS interfaces.

4.4.1. Schottky−Mott Limit. The barrier height at Schottky interfaces results from the charge exchanges required for Fermi-level equilibration. The majority of barrier heights for Schottky contacts with more than submonolayer metal coverage have shown values lying between the Mott−Schottky limit ($S = 1$) and the Bardeen limit ($S = 0$). When chemical bonding is neglected, the Mott−Schottky limit is expected when the charge balance is given by

$$Q_{IS} + Q_M = 0 \tag{11}$$

where Q_{IS} and Q_M refer to the amount of charge required to be transferred across the IS and metal interfaces, respectively. In the Mott−Schottky theory, the height of the zero bias interfacial potential barrier, ϕ_{b0}, is given for a Schottky interface by

$$q\phi_{b0} = |q\phi_m - E_X| \tag{12}$$

where E_X is the conduction (valence) band edge for an n-type (p-type) semiconductor and ϕ_m is the metal work function.[10] Equation 12 can also be generalized beyond metals by replacing $q\phi_m$ with $\bar{\mu}$ or qE of the contact as long as care is taken to refer all of the values to the same energy scale.

The ideal eq 12 is known as the Schottky−Mott limit and predicts $S = 1$. Experimentally, it is generally found for small band-gap semiconductors ($E_g < 2$ eV) that the barrier height is a less sensitive function of ϕ_m than eq 12 would suggest. In some cases, ϕ_b is nearly independent of ϕ_m, a situation termed Fermi-level pinning. Indeed, Tersoff noted that for the more covalent semiconductors, such as InP, the barrier height was independent of metal to within ±0.1 eV.[34] For InP|metal Schottky junctions, the average interface index is $S = 0.003$ for p-type,[35,36] and $S = 0.02$ for n-type.[37] As reported above, we have determined that S as extracted from the dependence of ϕ_b^{CV} on E_{PMH} for the InP|PMH interface is $S = 0.38 \pm 0.03$. Therefore, we conclude that a pronounced dependence of ϕ_{b0} on E_{PMH} exists at both the n-InP|PMH and p-InP|PMH interfaces, a situation not encountered at InP|metal Schottky contacts.

The ideal metal-semiconductor theory, as given in eq 11, assumes that there is no interaction between the two materials, nor is there an interfacial layer. For a real interface, however, chemical reactions between the contact and the semiconductor

can alter the ϕ_b, as do interfacial layers and interface states at the surface of the IS. Indeed, virtually all theoretical models involving Fermi-level pinning have concluded that at an IS|M interface, the Fermi level is pinned by states intrinsic to the interface.[38] Although most Fermi-level pinning models rely on the presence of some type of interface state, both the origin of these states and their number density are objects of considerable controversy.

4.4.2. Interface State Models. A variety of models have been proposed to explain the origin of states existing within the gap, including, but not limited to: metal induced gap states (MIGS), disorder induced gap states (DIGS), and defect states. These popular models assume that the interface states at a MS interface are a property of only the IS and not the metal and, consequently, that the interface states equilibrate with the semiconductor Fermi level. As is discussed further below and elsewhere,[33,39] any model based on interface states that equilibrate with the semiconductor cannot predict the near unity ideality factors often reported. Primarily due to the prevalence of interface state models in the literature, in this section we analyze our observed S value to calculate both an apparent density of states and an apparent neutrality level in order to discuss their relation to the predictions of the MIGS model and to the ideality factor. The term apparent is to emphasize that these values only have meaning if the observed Fermi-level pinning is truly due to interface states.

In the case where the polymer and the semiconductor remain separated by a thin insulating layer, and there is a continuous distribution of states present at the interface between the semiconductor and the insulator, characterized by a neutrality level ϕ_0, the barrier ϕ_b is predicted to be less sensitive to the work function of the contact. The neutrality level ϕ_0 is the position that the Fermi level must assume for the interface states to be uncharged. If states below ϕ_0 are empty, then the interface states have a net positive charge while if states above ϕ_0 are full, the interface states retain a net negative charge. For an IS|metal interface, the proposed relationship between the flat band barrier height, ϕ_b^0, and the work function of the metal ϕ_m is given as[40]

$$\phi_b^0 = \gamma(\phi_m - \chi_s) + (1 - \gamma)(E_g - \phi_0) \tag{13}$$

where

$$\gamma = \frac{\epsilon_i}{\epsilon_i + q\delta D_S} \tag{14}$$

and ϕ_0 is measured from the top of the valence band, D_S is the density of interface states per unit area per electronvolt (assumed constant), ϵ_i is the permittivity of the interfacial layer, and δ is the width of the interfacial layer. As above, eq 13 is readily generalized beyond metal contacts, and ϕ_m can be replaced by $\bar{\mu}$ or E as long as a consistent energy scale is used. The value of ϵ_i for various oxides on InP is estimated to be on the order of 2−5,[41] while 25 Å has been assumed as an upper limit for δ for an InP|PMH interface.[25] Furthermore, the parameter γ is often identified with the interface index S. In this manner, both the apparent density of interface states and the apparent neutrality level can be calculated based on the degree of pinning observed in the system. For the InP|PMH system, D_S is estimated to be between 8.0×10^{12} to 4.0×10^{13} states cm^{-2} eV^{-1}, for δ values of 10−20 Å, and ϵ_i values between 2 and 5, and under the assumption that the Fermi-level pinning is due to the presence of interface states. The apparent neutrality level, ϕ_0, for the n-InP|PMH and p-InP|PMH interfaces can be estimated by considering the saturated calomel electrode (SCE) to be −4.7 eV vs vacuum,[42] and by plotting the experimental ϕ_b values and those expected from the Mott−Schottky relationship versus E_{PMH}. The intersection of the two data sets is thus determined to be the apparent neutrality level of the interface. Such a comparison yields an apparent neutrality level of −5.15 eV versus vacuum for the p-InP|PMH system and −5.18 eV versus vacuum for the n-InP|PMH system, or approximately midgap. Again, these values and the concept of a neutrality level assume Fermi-level pinning due to interface states. For comparison, the conduction and valence band edge positions of InP at room temperature are −4.4 and −5.7 eV versus vacuum, respectively.[43] The similarity in the apparent neutrality levels calculated for the two semiconductors indicates that if the Fermi-level is being pinned by a density of interfacial states, both the n-InP|PMH and p-InP|PMH interfaces are being pinned by the same states. In this situation, the ϕ_b for the n-InP|PMH and p-InP|PMH interfaces at a given E_{PMH} should sum to the band gap. As shown in Figure 8, the average band gap extracted by using the sum of the two functions plotted is 1.36 ± 0.01 eV, which is consistent with the literature value of 1.37 eV for the band gap of indium phosphide at 248 K.

A central tenant of many interface state models used to describe Fermi-level pinning is that the interface states are a property of only the IS and not the contact. This is necessary, for instance, in the treatment of IS|metal Schottky diodes where interfaces based on different metals are all analyzed collectively to extract a single density of interface states. The large difference between the S value observed at the InP|PMH interface and that at Schottky interfaces based on InP argues that if interface states are important in determining ϕ_b at semiconductor interfaces, they must depend on the contact and consequently do not provide a general explanation for the relation between ϕ_b and $\bar{\mu}$ for all interfaces based on a particular semiconductor.

Relation between S and n_{emp}. As was previously stated, Card and Rhoderick discussed the implications of interface states equilibrating with the semiconductor or with the contact and derived an expression for the empirical ideality factor based on the density of interface states equilibrated with the semiconductor, D_{sb}, the density of interface states equilibrated with the contact, D_{sa}, the thickness δ of the interfacial layer, the depletion width W, and the permittivities ϵ_s and ϵ_i of the semiconductor and interfacial layer, respectively:[40]

$$n_{emp} = 1 + \frac{\left(\frac{\delta}{\epsilon_i}\right)\left(\frac{\epsilon_s}{W} + qD_{sb}\right)}{1 + \left(\frac{\delta}{\epsilon_i}\right)qD_{sa}} \tag{15}$$

Three limiting cases of eq 15 are of interest:

(I) If the density of interface states is sufficiently small so as not to influence the potential distribution, eq 15 becomes

$$n_{emp} = 1 + \frac{\delta\epsilon_s}{W\epsilon_i} \tag{16}$$

(II) If all of the interface states equilibrate with the contact, that is $D_{sb} \rightarrow 0$, eq 15 reduces to

$$n_{emp} = 1 + \frac{\delta\epsilon_s}{W(\epsilon_i + \delta qD_{sa})} = 1 + \frac{\delta\epsilon_s}{W\epsilon_i} \tag{17}$$

(III) If all of the interface states equilibrate with the semiconductor, that is $D_{sa} \rightarrow 0$, eq 15 reduces to

$$n_{emp} = 1 + \frac{\delta}{\epsilon_i}\left(\frac{\epsilon_s}{W} + qD_{sb}\right) = \frac{1}{S} + \frac{\delta\epsilon_s}{\epsilon_i W} \qquad (18)$$

The dependence on D_{sa} and D_{sb} can be understood physically because states in equilibrium with the contact tend to hold ϕ_b constant (i.e., to reduce n_{emp}) while states in contact with the semiconductor tend to hold V_b constant (i.e., to increase n_{emp}).

For states equilibrating with the semiconductor, filling is determined by the applied bias. Since the filling of these states determines the point at which the semiconductor band edges are fixed at the interface, and consequently, the barrier height, the barrier depends on applied bias. This condition therefore leads to ideality factors greater than unity. This can be seen in eq 18, where Card and Rhoderick's expression has been rewritten in terms of the interface index S. For $S = 0.39$, as observed herein, eq 18 predicts $n_{emp} \geq 2.5$.

The filling of interface states equilibrating with the contact Fermi level is not perturbed by the applied bias, and the ideality factor does not substantially deviate from unity for a thin interfacial layer, as evidenced by eq 17. The observation of our near unity ideality factors at room temperature suggests that if interface states are pinning the interface, they equilibrate with the PMH. The presence of an interfacial layer and interface states would not be surprising given the fact that the InP|PMH interfaces were fabricated in air by using an oxidative polymerization, and there is evidence for distinct surface interactions from SEM data. As a general explanation of the dependence of ϕ_b on $\bar{\mu}$, however, interface states equilibrating with the contact implies that their density should depend sensitively on the contact chosen. This is at odds with general theories of Fermi-level pinning that invoke interface states that depend only on the IS. This apparent discrepancy can be reconciled in the context of the chemical bonding model discussed below.

Due to its prevalence, it is also interesting to specifically compare the observations at for the InP|PMH interface to the predictions of the MIGS model. Heine identified Bardeen's continuum of gap states as exponentially decaying tails of metal wave functions derived from the continuum of virtual gap states of the complex semiconductor band structure.[44] Tejedor and Flores pointed out that the MIGS (as they were later called) tend to pin the Fermi level at the "neutrality point" of the interface to maintain local charge neutrality in the semiconductor in the region where MIGS have significant amplitude.[45] Tersoff calculated this neutrality point for InP as −4.92 eV versus the vacuum level.[46] Indeed, both n-InP|PMH and p-InP|PMH interfaces are pinned at −5.17 eV versus vacuum, which is approximately midgap. Monch has made a theoretical prediction of the interface index S based on the MIGS model.[47] This prediction gave the following relationship for S:

$$S = \left[1 + 0.29\frac{(\epsilon_\infty - 1)^2}{\epsilon_i}\right]^{-1} \qquad (19)$$

where ϵ_i is the interface dielectric constant and ϵ_∞ is the electronic portion of the static dielectric constant. With $\epsilon_i = 4$ and $\epsilon_\infty = 9.61$, an S value of 0.16 is obtained. The interface index of 0.38 reported in this paper for InP|PMH interfaces indicates a much stronger dependence on contact work function (or E_{PMH}) than that proposed by the MIGS model.

4.4.3. Chemical Bonding Model. Recently, Tung questioned the idea that gap states are responsible for Fermi-level pinning and asserted instead that chemical bonding is the primary mechanism of the Schottky barrier height.[39] He pointed out several discrepancies between the MIGS model and experimental observations. For instance, epitaxial MS interfaces have shown that the Schottky barrier height depends on interfacial atomic structure,[48,49] while the MIGS model predicts no such dependence on orientation. Furthermore, as was pointed out above, near unity ideality factors found in the literature cannot be reconciled with gap states which equilibrate with the semiconductor. It was for these reasons that Tung concluded that although MIGS are present at every MS interface, they do not lead to an interface dipole in the fashion assumed by existing models.

The observation that changes in the interface structure have been shown to effect ϕ_b suggests that the Schottky barrier height likely depends sensitively on the choice of metal, in conflict with the observation of Fermi-level pinning found in the literature. In place of the gap states models, Tung proposed that chemical bonding determines the Schottky barrier height characteristics. Specifically, when a metal comes into contact with an IS, chemical bonding takes place, setting up an interfacial dipole. Using a simple model of bond polarization, Tung calculated the voltage drop across this dipole layer and determined the form of the Schottky barrier height as given here:

$$\phi_{b,n}^0 = \gamma_B(\phi_M - \chi_S) + (1 - \gamma_B)\frac{E_g}{2} \qquad (20)$$

$$\gamma_B = 1 - \frac{q^2 d_{MS} N_B}{\epsilon_{IT}(E_g + \kappa_H)}$$

where κ_H is the sum of all the hopping interactions, d_{MS} is the distance between the metal and semiconductor atoms at the interface, N_B is the density of chemical bonds assumed to form across the interface, ϵ_{IT} is the interface dielectric constant, and γ_B can be thought of as the familiar interface index S. This equation predicts a dependence of the Schottky barrier height on metal work function, but it is the polarization of the chemical bonds at the interface, rather than the filling of gap states, which is responsible for this weak dependence. This model also predicts that the SBH should naturally converge toward the middle of the band gap of the IS, as is seen in both the n-InP|PMH and p-InP|PMH systems.

When the chemical bonding model is considered in the context of IS|DCP interfaces, some additional attributes of doped conjugated polymers should be noted. The PMH oxidative polymerization is done directly on the semiconductor surface. As presented in section 3.5, SEM micrographs of sectioned InP|PMH interfaces have indicated the presence of a molybdenum rich layer at the interface between the indium phosphide and the PMH. The presence of such a layer suggests some degree of interfacial reactivity. Nonetheless, when compared with IS|M interfaces, the molecular nature of the PMH implies an absence of surface dangling bonds, thereby minimizing the potential for interfacial reactions relative to metals. Within the surface bonding model, reduced interfacial reactivity (a smaller number of interfacial bonds N_B) should lead to a less pinned system. Although a relatively simplistic model, the higher S values observed at the InP|PMH interface relative to InP|metal interfaces is consistent with the notion of weaker chemical interactions as reflected in Tung's model through a smaller value of N_B. It is also consistent with the observation that the Schottky−Mott limit ($S = 1$) has been achieved at interfaces between silicon and small molecule liquid redox couples that are relatively unreactive[50] and also appears to be approached for metals on certain low-dimensional layered semiconductors, such as WSe_2.[51]

4.5. Relation of κ to E_{PMH}. Figure 10 summarizes the dependence of κ on E_{PMH} for both n-InP|PMH and p-InP|PMH interfaces. The recognition of κ_θ^{CV} as an upper limit and κ_θ^{RP} as a lower limit (section 4.2.3)[29] is important in interpreting this figure. For n-InP|PMH interfaces, κ_θ^{CV} and κ_θ^{RP} generally agree to within experimental error, and κ is estimated to be approximately 0.003 and independent of temperature. For p-InP|PMH interfaces, the general trend is for κ to decrease from the range of 1−0.1 to the range 0.05−0.001 as E_{PMH} increases. The scatter in the data and the disagreement between κ_θ^{CV} and κ_θ^{RP} highlight the difficulties in calculating κ with accuracy much better than an order of magnitude. Viewed in terms of the driving force for carrier transfer, κ increases as the driving force for hole transfer increases at the p-InP|PMH interfaces, and it remains relatively small for the n-InP|PMH interfaces despite the large driving forces realized. Here, the driving force for carrier transfer is identified as the difference between the relevant band edge and the equilibrium $\bar{\mu}$ characterizing the interface, as measured by ϕ_b.

The results for κ are qualitatively in agreement with expectations regarding the density of states of the PMH. For inorganic semiconductor (IS)|metal (M) interfaces, it is assumed that every electron with sufficient energy to surmount the interfacial potential barrier and that is coincident with the metal surface is collected by the metal, corresponding to the limit $\kappa \rightarrow 1$. However, at molecular IS interfaces, values of κ often much less than one have been observed.[13,50] For some interfaces, values of κ less than unity have often been attributed to the presence of an interfacial layer, where κ is exponentially related to the thickness and potential barrier of the layer.[40] In contrast, the transition probability for liquid redox couples has been proposed to follow Fermi's golden rule equation, with a dependence on the density of states (DOS) and the interaction potential.[52]

The density of states for PMH is expected to be lower than that of a metal, and this is consistent with the general observation of $\kappa < 1$. In the voltammetry of PMH, the p-doping wave for the polymer, which can be considered as accessing the HOMO states or the valence band, is a broad wave extending well over 1 V positive of −0.1 V vs SCE. Considering SCE to be −4.7 V vs vacuum and the difference in sign convention between the electrochemical scale and the absolute energy scale, the HOMO or valence band edge of PMH is estimated to be in the vicinity of −4.6 V vs vacuum, and the region of electroactivity extends negative to beyond −6 V. Of course, it is difficult to precisely know band edge alignments from voltammetry data; nonetheless, these observations can be used to qualitatively rationalize the observed dependence of κ on E_{PMH}. The voltammetry data suggests that the conduction band edge (−4.4 V vs SCE) of InP lies in a region where the PMH is not electroactive, signaling a low density of available states; whereas the valence band edge (−5.7 V vs SCE) lies in a region where the polymer is electroactive, signaling a higher density of available states. This difference in density of states is consistent with κ for the n-InP|PMH interfaces being lower than for p-InP|PMH interfaces. It is also consistent with a stronger dependence on E_{PMH} because electrochemical manipulation is expected to more strongly influence the states accessible to the valence band. More rigorous interpretation of these data requires photoelectron measurements to better assess the relevant band edge alignments. It is also noted that mediation of electron transfer by interface states has not been ruled out. An influential interfacial layer or interface states clouds the direct correlation of current density with the true heterogeneous charge-transfer rate, thereby complicating any interpretation in terms of band edge density-of-states profiles.

4.6. Quantitative Modeling of Current−Voltage Characteristics: Barrier Inhomogeneity Model. The focus of this discussion now shifts to the quantitative modeling of the current−voltage characteristics of the InP|PMH interfaces. To explain commonly observed deviations from classic TE theory, Tung has treated a system of barrier inhomogeneities or "patches" imbedded in a background of uniform barrier height, $q\phi_{b0}$, which is independent of applied potential.[27] The patches are taken to be small relative to the depletion region that exists within the IS such that the interaction of the patch with the surrounding depletion region causes a "pinch-off" or saddle point in the potential barrier away from the interface. For circular patches, Tung introduced a strength parameter $\gamma = 3(R_o^2\Delta_o/4)^{1/3}$ collectively describing the radius of these patches, R_0, and their nominal barrier height, $q\phi_{b,patch} = q(\phi_{b0} - \Delta_0)$, relative to the higher barrier uniform background, $q\phi_{b0}$, where Δ_0 is the decrease in the barrier at the interface in the presence of a patch. The effective barrier for transport is defined by a saddle point potential removed from the interface and is increased relative to $q\phi_{b,patch}$ due to potential pinch-off.

The $J-V_{app}$ relation in the presence of a distribution of small, low-density circular patches is given by

$$J' = \kappa A^* T^2 \exp[\beta(V_{app} - \phi_{b0})](1 + \zeta) \qquad (21)$$

where ζ depends on the density c and strength factors γ of the patches, as well as V_{app} and temperature. In effect, eq 21 represents two currents: one from the usual thermionic emission over a homogeneous barrier and an additional correction current due to majority carrier transport through the patches.

More quantitatively, if the strength factor γ has a half-Gaussian distribution for $\gamma \geq 0$, ζ has the form

$$\zeta = \frac{8\pi c\sigma^2}{9}\left(\frac{\eta}{V_b}\right)^{1/3} \exp\left[\frac{\beta^2\sigma^2}{2}\left(\frac{V_b}{\eta}\right)^{2/3}\right] \qquad (22)$$

where σ is the standard deviation of the strength parameter γ about zero and $\eta = \epsilon_s/qN_A$. With the assumption that κ has no voltage or temperature dependence, the result of fits over a constant J' range for both an n-InP|PMH and p-InP|PMH interface is shown in Figure 12 with κ, σ, and c as parameters. In this fit, the background barrier ϕ_{b0} was taken as the temperature-dependent ϕ_b^{CV}. The extent to which the patch model can represent the temperature-dependent $J'-V_{app}$ data using the ϕ_b^{CV} represents the extent to which it consistently explains the apparent anomalies observed between $C-V_{app}$ and RP measurements. The average values of reduced χ^2 for the n-InP|PMH interfaces (0.04) relative to the p-InP|PMH interfaces (0.10) indicates that a better fit was achieved for the n-InP|PMH interfaces. The fits were also in general poorer than for as-synthesized interfaces.

The parameters σ and c showed no clear trend with E_{PMH}. The average values for the parameters for all of the n-InP|PMH interfaces are $\sigma = 5.76 \times 10^{-5}$ V$^{1/3}$ cm$^{2/3}$ and $c = 1.36 \times 10^{11}$ cm^{-2}, as compared to the average for all of the p-InP|PMH interfaces with $\sigma = 2.94 \times 10^{-5}$ V$^{1/3}$ cm$^{2/3}$ and $c = 5.39 \times 10^{12}$ cm^{-2}. Furthermore, for both the n-and p-InP|PMH interfaces, the average patch density was observed to be approximately an order of magnitude higher than the surface dopant density (for n-InP the surface dopant density is $N_D^{2/3} = 3.0 \times 10^{10}$ and for p-InP, $N_A^{2/3} = 1.2 \times 10^{11}$ cm^{-2}). Assuming that the patch parameter Δ_0 is constant, one can then calculate

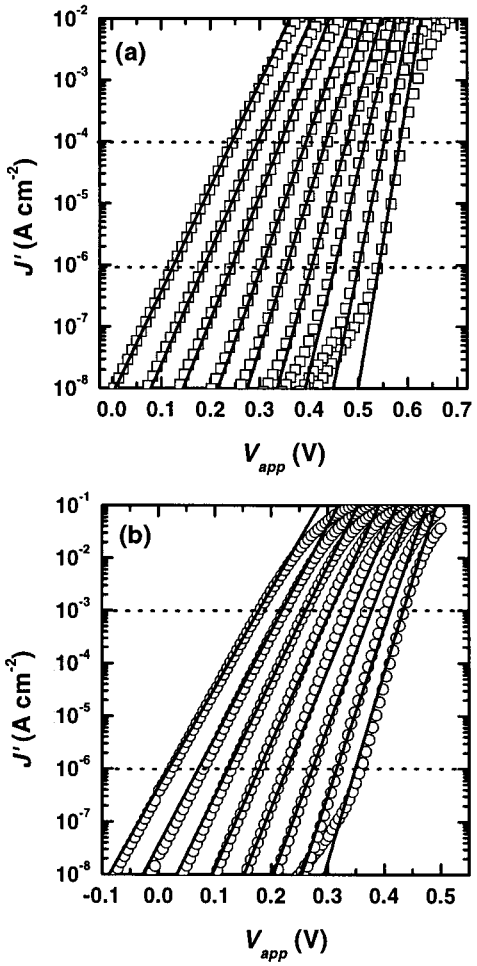

Figure 12. Temperature dependence of the reduced current density J' for (a) interface n5 (n-InP|PMH) for temperatures ranging from 98 to 298 K, stepped by 25 K and for (b) interface p5 (p-InP|PMH) for temperatures ranging from 108 to 248 K, stepped by 20 K. Every other data point at each temperature is shown for clarity. The solid lines represent a fit to Tung's model for a half-Gaussian distribution of lower barrier patches (eq 26) with best-fit parameters: $\kappa = 9.28 \times 10^{-4}$, $\sigma = 4.20 \times 10^{-5}$ V$^{1/3}$ cm$^{2/3}$, and $c = 1.05 \times 10^{11}$ cm^{-2} for interface n5, and $\kappa = 0.015$, $\sigma = 3.65 \times 10^{-5}$ V$^{1/3}$ cm$^{2/3}$, and $c = 1.13 \times 10^{12}$ cm^{-2} for interface p5. The horizontal dotted lines bound the range of J' over which the modeling was undertaken.

the area of coverage by lower barrier patches by integrating the area of the patches over the distribution of γ's. The fractional area f_p of coverage for a half-Gaussian ($\gamma > 0$) distribution is thus

$$f_p = \sqrt{2\pi}\frac{c}{\sigma}\int_0^\infty {R_0}^2 \exp[-\gamma^2/2\sigma^2]\, d\gamma \qquad (23)$$

If it is assumed that Δ_0 is 0.75 of $\phi_b^{CV}(T{=}248\text{ K})$ then the value of f_p for the n-InP|PMH interfaces is generally calculated to be 3%, while that of the p-InP|PMH interfaces is generally calculated to be 30%. These values were derived with a relatively large value of Δ_o. Any smaller value of Δ_o would result in an even larger surface coverage. An assumption of the model used is that the patches are independent of each other. Given the large f_p, in particular for the p-InP|PMH interfaces, this assumption may not be valid, and unaccounted interactions between patches may help explain why the modeling was less successful for p-InP|PMH interfaces.

The dependence of κ on E_{PMH} observed from fitting the $J'-V_{app}$ was similar to that inferred from the upper and lower limits

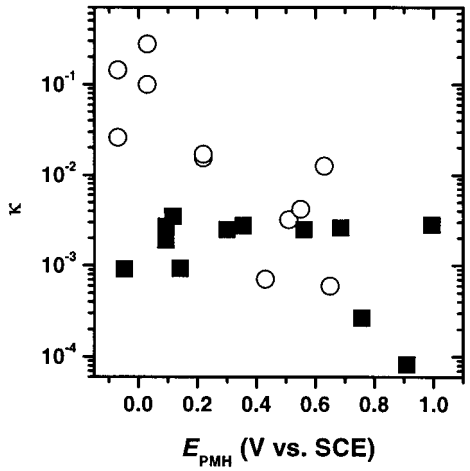

Figure 13. Best fit values of κ as a function of E_{PMH} for the n-InP|PMH (squares) and p-InP|PMH (circles) interfaces studied. The values of κ were derived from a fit to Tung's barrier inhomogeneity model with a half-Gaussian distribution of barrier inhomogeneities.

ϕ_b^{CV} and ϕ_b^{RP}, respectively. Figure 13 shows the best-fit values of κ as a function of E_{PMH}. For the n-InP|PMH interfaces, the best fit κ is found to be relatively independent of E_{PMH}, although there are two decidedly lower values; the average value of $\kappa = 0.002$ is in good agreement with that estimated from κ_θ^{CV} and κ_θ^{RP}. For the p-InP|PMH interfaces, the best-fit κ decreases with increasing E_{PMH} as inferred from the upper and lower limits above with κ more closely following the lower limit trend.

Although the qualitative indications of barrier heterogeneity are present in both the n-InP|PMH and p-InP|PMH interfaces, as discussed in section 4.1, the quantitative modeling of the $J'-V_{app}$ characteristics of these interfaces did not hold as rigorously as that of the as-synthesized interfaces. Nevertheless, the ability of the barrier inhomogeneity model to qualitatively explain the temperature dependence of n_{emp}, as well as the nonphysicality of some calculated values of κ, and the deviation of the $J-V_{app}$ and $C-V_{app}$ measured barrier heights is compelling.

5. Summary

We have completed a detailed study of the current−voltage and capacitance voltage characteristics of the interface between InP and a polypyrrole phosphomolybdate hybrid material (PMH) as a function of the redox potential of the PMH, E_{PMH}. Through electrochemically manipulating E_{PMH} over a range where it remains a good conductor, it is possible to continuously tune the current−voltage characteristics of the interface. In the case of n-InP|PMH interfaces, the control is exclusively due to controlling the interfacial potential barrier ϕ_b, whereas, for the p-InP|PMH interfaces, the control arises from a change in both the transmission coefficient κ and ϕ_b.

The magnitude of the change in the spatially averaged ϕ_b with E_{PMH} was found to be the same for both n-InP|PMH and p-InP|PMH interfaces, yielding an index of interface behavior of $S = 0.38$. This value of S is much higher than observed at InP|metal interfaces ($S < 0.1$), but still substantially less than the ideal Schottky−Mott limit. The dependence of S on the nature of contact, metal vs PMH, demonstrates that the central assumption of classic interface state models describing Fermi-level pinning is not general; the greater control over ϕ_b possible at the InP|PMH interface relative to InP|metal interfaces demonstrates that ϕ_b is not in general controlled by a density of interface states *intrinsic* to the semiconductor. This does not,

however, rule out the possibility that interface states are responsible for limiting S below the Schottky−Mott limit. Any such states, however, are likely characteristic of the interfacial chemistry unique to the InP|PMH interface rather than an intrinsic property of the InP, and such chemistry may be better discussed in terms of models more directly relating to chemical bonding and the formation of surface dipoles, such as that proposed by Tung.[39]

In particular for the p-InP|PMH interfaces, the extraction of transmission coefficients κ, is complicated by disagreement between different techniques for measuring the barrier and from transport behavior that does not rigorously follow ideal TE. These anomalies were treated in terms of a heterogeneous barrier potential allowing for the extraction of upper and lower limits on κ. The results indicate that κ for the n-InP|PMH interfaces is substantially below the semiconductor|metal limit of unity and independent of E_{PMH}, whereas for the p-InP|PMH interfaces, κ decreases from near unity to values typical of the n-InP|PMH interfaces as E_{PMH} increases. Quantitative modeling using Tung's barrier inhomogeneity model further supported these results. The trends in κ suggest that the electronic density of states in the PMH may limit the heterogeneous charge transfer rate, although mediation by an interfacial layer/states cannot be ruled out. Photoelectron studies are needed to more clearly map out the density of states profile of the PMH and the band edge alignments at the InP|PMH interface. The dependence of κ on E_{PMH} also emphasizes that the index of interface behavior describing the shift in ϕ_b with electrochemical potential cannot be extracted from the shifts in current−voltage curves alone.

Acknowledgment. We acknowledge the Beckman Young Investigator Awards Program, the National Science Foundation (CAREER, DMR-9703311), the Dreyfus Foundation New Faculty Awards Program, and the University of Oregon for their generous support. C.D-H. acknowledges the U.S. Department of Education for receipt of a GAANN fellowship. We also acknowledge Frank Jones for his help in preparing this manuscript.

References and Notes

(1) Freund, M. S.; Karp, C.; Lewis, N. S. *Inorg. Chim. Acta* **1995**, *240*, 6.
(2) Gomez-Romero, P.; Lira-Cantu, M. *Adv. Mater.* **1997**, *9*, 3.
(3) Lonergan, M. C. *Science* **1997**, *278*, 2103.
(4) Inganas, O.; Skotheim, T.; Lundstrom, I. *J. Appl. Phys.* **1983**, *54*, 3636.
(5) Frank, A. J.; Glenis, S.; Nelson, A. J. *J. Phys. Chem.* **1989**, *93*, 3818.
(6) Sailor, M. J.; Klavetter, F. L.; Grubbs, R. H.; Lewis, N. S. *Nature* **1990**, *346*, 155.
(7) Greenham, N. C.; Friend, R. H. Semiconductor Device Physics of Conjugated Polymers. In *Solid State Physics: Advances in Research and Applications*; Ehrenreich, H., Spaepen, F., Eds.; Academic Press: New York, 1995; Vol. 49, p 1.
(8) Sikes, H. D.; Smalley, J. F.; Dudek, S. P.; Cook, A. R.; Newton, M. D.; Chidsey, C. E. D.; Feldberg, S. W. *Science* **2001**, *291*, 1519.
(9) Wilmsen, C. W. *Physics and chemistry of III−V compound semiconductor interfaces*; Plenum Press: New York, 1985.
(10) Rhoderick, E. H.; Williams, R. H. *Metal-Semiconductor Contacts*, 2nd ed.; Oxford University Press: Oxford, U.K., 1988; Vol. 19.
(11) Monch, W. *Semiconductor Surfaces and Interfaces*, 2nd ed.; Spring-Verlag: Berlin, 1995; Vol. 26.
(12) Marcus, R. A. *J. Phys. Chem.* **1990**, *94*, 1050.
(13) Lewis, N. S. *Annu. Rev. Phys. Chem.* **1991**, *42*, 543.
(14) Nozik, A. J.; Memming, R. *J. Phys. Chem.* **1996**, *100*, 13061.
(15) Gao, Y. Q.; Georgievskii, Y.; Marcus, R. A. *J. Chem. Phys.* **2000**, *112*, 3358.
(16) Parkinson, B. *Acc. Chem. Res.* **1984**, *17*, 431.
(17) Gerischer, H. Semiconductor Electrochemistry. In *Physical Chemistry an Advanced Treatise*; Eyring, H., Henderson, D., Jost, W., Eds.; Academic: New York, 1970; Vol. 9A.
(18) Koval, C. A.; Howard, J. N. *Chem. Rev.* **1992**, *92*, 411.
(19) Tan, M. X.; Laibinis, P. E.; Nguyen, S. T.; Kesselman, J. M.; Stanton, C. E.; Lewis, N. S. *Prog. Inorg. Chem.* **1994**, *41*, 21.
(20) Kumar, A.; Wilisch, W. C. A.; Lewis, N. S. *Crit. Rev. Solid State Mater.* **1993**, *18*, 327.
(21) Fajardo, A. M.; Lewis, N. S. *Science* **1996**, *274*, 969.
(22) Bethe, H. A. MIT Radiation Lab. Rep. 1942.
(23) Sze, S. M. *Physics of Semiconductor Devices*; Wiley: New York, 1981.
(24) Jones, F. E.; Daniels-Hafer, C.; Wood, B. P.; Danner, R. G.; Lonergan, M. C. *J. Appl. Phys.* **2001**, *90*.
(25) Jones, F. E.; Wood, B. P.; Myers, J. A.; Daniels-Hafer, C.; Lonergan, M. C. *J. Appl. Phys.* **1999**, *86*, 6431.
(26) Our stoichiometry for the synthesis of PMH is slightly different from that of Gomez-Romero and Lira-Cantu. Elemental analysis on our PMH performed by Robertson Microlit Laboratories, Inc. found, C 18.74%, H 1.86%, N 5.42%, Mo 46.50%, P 1.26%. Gomez-Romero and Lira-Cantu proposed a formula of $(C_4H_3N)_x[PMo_{12}O_{40}]^{3\ominus}$ with $x = 9$; our results are qualitatively consistent with this formulation, and $x = 9.3$ yields, Calc. C 17.96%, H 1.13%, N 5.24%, Mo 47.81%, P 1.29%. Cyclic voltammetry on our PMH is also in agreement with that reported by Gomez-Romero and Lira-Cantu.
(27) Tung, R. T. *Phys. Rev. B* **1992**, *45*, 13509.
(28) Kuphal, E. *Solid-St. Electron.* **1981**, *24*, 69.
(29) Lonergan, M. C.; Jones, F. E. *J. Chem Phys.* **2001**, *114*.
(30) Missous, M.; Rhoderick, E. H. *J. Appl. Phys.* **1991**, *69*, 7142.
(31) As discussed by Missous and Rhoderick,[30] this is not necessarily the true zero Kelvin barrier but a "notional" value calculated by extrapolation from finite temperatures.
(32) Sullivan, J. P.; Tung, R. T.; Pinto, M. R. *J. Appl. Phys.* **1991**, *70*, 7403.
(33) Freeouf, J. L. *Appl. Phys. Lett.* **1982**, *41*, 285.
(34) Tersoff, J. *Phys. Rev. Lett.* **1984**, *52*, 465.
(35) Chen, W. X.; Yuan, M. H.; Wu, K.; Zhang, Y. X.; Wang, Z. M.; Qin, G. G. *J. Appl. Phys.* **1995**, *78*, 584.
(36) Newman, N.; Van Schilfgaarde, M.; Spicer, W. E. *Phys. Rev. B: Condens. Matter* **1987**, *35*, 6298.
(37) Newman, N.; Kendelewicz, T.; Bowman, L.; Spicer, W. E. *Appl. Phys. Lett.* **1985**, *46*, 1176.
(38) Tersoff, J. *NATO ASI Ser., Ser. B* **1989**, *195*, 281.
(39) Tung, R. T. *Phys. Rev. Lett.* **2000**, *84*, 6078.
(40) Card, H. C.; Rhoderick, E. H. *J. Phys. D* **1971**, *4*, 1589.
(41) Lee, Y. S.; Anderson, W. A. *J. Appl. Phys.* **1989**, *65*, 4051.
(42) Reiss, H.; Heller, A. *J. Phys. Chem.* **1985**, *89*, 4207.
(43) Shmidt, N. M. *Handbook series on semiconductor parameters*; Levinshtein, M. E., Ed.; World Scientific: Singapore London, 1996; Vol. 1, p 169.
(44) Heine, V. *Phys. Rev.* **1965**, *138*, A 1689.
(45) Tejedor, C.; Flores, F.; Louis, E. *J. Phys. C* **1977**, *10*, 2163.
(46) Tersoff, J. *J. Vac. Sci. Technol., B* **1985**, *3*, 1157.
(47) Monch, W. *Appl. Surf. Sci.* **1996**, *92*, 367.
(48) Heslinga, D. R.; Weitering, H. H.; van der Werf, D. P.; Klapwijk, T. M.; Hibma, T. *Phys. Rev. Lett.* **1990**, *64*, 1589.
(49) Tung, R. T. *Phys. Rev. Lett.* **1984**, *52*, 461.
(50) Fajardo, A. M.; Lewis, N. S. *J. Phys. Chem. B* **1997**, *101*, 11136.
(51) Jaegermann, W.; Pettenkofer, C.; Parkinson, B. A. *Vacuum* **1990**, *41*, 800.
(52) Royea, W. J.; Fajardo, A. M.; Lewis, N. S. *J. Phys. Chem. B* **1997**, *101*, 11152.